

## Mineralogical and geochemical investigation of clay-rich mine tailings from a closed phosphate mine, Bartow Florida, USA

Mark P. S. Krekeler · Julie Morton · Jill Lepp ·  
Cynthia M. Tselepis · Mikhail Samsonov ·  
Lance E. Kearns

Received: 20 June 2007 / Accepted: 28 July 2007 / Published online: 11 October 2007  
© Springer-Verlag 2007

**Abstract** Clay-rich mine tailings from phosphate mine operations in Florida are a major environmental and economic problem. Options for reclamation and restoration for these tailings are very limited and are fundamentally restricted by poor physical properties such as low mechanical strength, low hydraulic conductivity, and heavy metal content. The major control on these bulk physical properties is the mineralogy of the materials. Eight continuous push borings were obtained to investigate stratigraphy, mineralogy, aspects of geochemistry, and bulk properties of a deposit of clay-rich mine tailings from a phosphate mine near Bartow, Florida that ceased operations in the early 1970s. Stratigraphy is dominated by laminated clay-rich sediment with minor units of silt and sand. An intact kaolinite liner occurs near the impoundment walls and the impoundment floor has approximately 4 m of relief. Moisture content varies from 4.35 to 57.40 wt% and organic content varies from 0.41 to 9.53 wt%. Bulk XRF investigation indicates that the  $P_2O_5$  concentrations vary from approximately 4 to 21 wt%. A very strong correlation ( $r^2 = 0.92$ ) between CaO and  $P_2O_5$  indicates that apatite is a major control on the phosphate. The strong correlation ( $r^2 = 0.77$ ) of  $Al_2O_3$  and  $TiO_2$  suggests that the source materials for this deposit are comparatively uniform. A number of heavy metal elements

and trace elements occur. Cr, V, Ni, Cu are interpreted to be in phosphate minerals, largely apatite. Sr and Pb are interpreted to be in both phyllosilicates and phosphate minerals. Two populations of apatite were observed in the clay-sized fraction, one that was Fe and Si-bearing and another that was only Si-bearing. Fe-bearing apatite had  $Fe_2O_3$  contents that varied from 0.38 to 5.32 wt% and  $SiO_2$  contents that varied from 0.90 to 3.32 wt%. The other apatite population had a wider range of  $SiO_2$  contents that varied from 0.77 to 8.80 wt%. TEM imaging shows that apatite grains are dominantly single crystals with lesser amounts of aggregates. Wavellite commonly occurs as individual or clusters of lath-like crystals and the chemical composition differs from the pure aluminium phosphate end member with average concentrations of components being that of CaO (1.57 wt%),  $Fe_2O_3$  (1.98 wt%),  $SiO_2$  (5.94 wt%). In the clay-sized phosphate minerals investigated no fluorine was found above detection limit (approximately 0.15 wt%), nor was any uranium, radium, heavy metal, or REE element detected. The phyllosilicate mineralogy of the deposit is dominated by smectite (montmorillonite with lesser amounts of nontronite), palygorskite, illite and kaolinite. No systematic variation in the relative proportions of phyllosilicates was observed in the clay deposit. Energy dispersive spectroscopy EDS analysis indicates that chemical compositions of phyllosilicates are somewhat typical but overall are enriched with respect to Fe compared to theoretical end members. The relative enrichment of Fe is interpreted to be a primary sedimentary feature. Ca content in smectite minerals is high and may inhibit stabilization using lime or similar methods. The high percentages of montmorillonite and palygorskite explain the high bulk water contents observed. This investigation provides fundamentally new details regarding clay tailing deposits from closed phosphate

---

M. P. S. Krekeler (✉) · J. Morton · J. Lepp ·  
C. M. Tselepis · M. Samsonov  
Department of Environmental Science and Policy,  
George Mason University, Fairfax, VA 22030, USA  
e-mail: mark.krekeler@gmail.com

L. E. Kearns  
Department of Geology and Environmental Sciences,  
James Madison University, MSC 7703,  
Harrisonburg, VA 22807, USA

mines in central Florida which can be used in restoration and reclamation efforts.

## Introduction

Phosphate is a key economic resource to which food production and the chemical industry is closely tied on a global scale. In the US alone 30.7 million tons of phosphate product with a value of approximately \$852 million are produced (Jasinski 2007). Florida is a leading phosphate producer with 75% of the U.S. production and 25% of world production (Brown 2005). Approximately 2,000 ha of land is mined in Florida each year for phosphate production and approximately 121,400 ha has been directly affected by mining (Brown 2005). Other major phosphate producers are China which has surpassed the U.S. in volume production in 2006, and Morocco, Tunisia and Russia (Jasinski 2007).

Phosphate mining poses a set of global environmental challenges including production of large amounts of waste, mine drainage problems and heavy metal pollution (e.g. Mendez et al. 2006; Ryser et al. 2005; Pierce et al. 2004; Fessler et al. 2003; Mars and Crowley 2003; Ghose 2003; Das 1999; Komnitsas et al. 1998). Such problems are evident in Florida. One of the most pressing environmental problems is mine waste generated from over a century of phosphate production. One ton each of waste sand and clay is produced for each ton of final phosphate product (Singh et al. 2006). The clay deposits and clay settling areas resulting from the waste are considered very problematic owing to difficulties in reclamation and restoration.

### Summary of mine waste and restoration

The mining process and waste streams for Florida operations have been described elsewhere (e.g., Ford et al. 1990; LaFevers et al. 1977). The Florida phosphate mining industry began in 1888, however, reclamation regulations only apply to lands directly affected by mining after July 1, 1975. According to Florida's Environmental Protection Bureau of Mine Reclamation's 2005 Rate of Reclamation Report, 73,000 ha of land were mined for phosphate between 1975 and 2005. Of the land affected by ore removal, only 64% is completely reclaimed to agricultural or industrial purposes.

Clay tailings are composed of both phyllosilicate and non-phyllosilicate minerals. The common phyllosilicate minerals include smectite (montmorillonite), kaolinite, illite, and palygorskite (Hawkins 1973; Zhang and Bogan 1995; Novich and Martin 1989; Shang and Lo 1997; Ford

et al. 1990; Vasan 1971). Other common minerals are apatite, quartz, feldspar, dolomite, millisite, and wavellite (Hawkins 1973; Zhang and Bogan 1995; Novich and Martin 1989; Shang and Lo 1997; Vasan 1971). The literature indicates that the proportions and presence of the above minerals varies significantly from one processing facility to another (Zhang and Bogan 1995; Novich and Martin 1989).

Restoration efforts for phosphate mines are in place (e.g., Andrews and Broome 2006; Brown 2005; Erwin et al. 1997). Modeled estimates of the time necessary to achieve full restoration for mines in Florida vary from 100 years if ecologically engineered practices are followed, to as much as 500 years for natural attenuation (Weber 1994; Brown 2005). However, long term management and ultimately the success of restoration efforts is in part dependent upon an understanding of the mineralogy and geochemistry of the clay materials. Ruston (1988) identified soil structure as a major factor in the effectiveness of restoration and noted that high phyllosilicate content and shrink swell properties make restoration efforts challenging. Detailed understandings of water content, mineral content and the nature of heavy metal distribution are important factors in long term ecological health of reclaimed systems.

Detailed investigations of the bulk properties and mineralogy of clay tailings deposits after deposition and aging are uncommon. Whether there is systematic variation in water content, mineral content, or bulk chemical composition is not known. The nature of stratigraphic variation within a deposit is also unknown. The mineralogic controls on bulk chemical composition of major, minor and trace elements are only partially understood as chemical analyses on discrete clay particles are lacking.

This investigation examines the variability of sediments, bulk properties, mineralogy, and bulk chemical composition of a representative deposit from a mine which ceased operations in the early 1970s in Polk County, Florida. To our knowledge this project is the first to conduct a detailed mineralogical study of cores obtained from such a deposit.

## Methods

The site area (approximately 27° 50.6 N, 081° 50.3 W) was heavily overgrown with dense vegetation making coring operations difficult and restricting the number and distribution of cores. Ten borings were attempted and eight borings were successfully advanced using direct-push Geoprobe<sup>®</sup> technology (Fig. 1). Soil cores were collected continuously (with the exception of the tops of cores 2 and 3) from the top of the clay, approximately 1.5–3.0 m below ground surface (bgs), to approximately 13.7 m (bgs) in

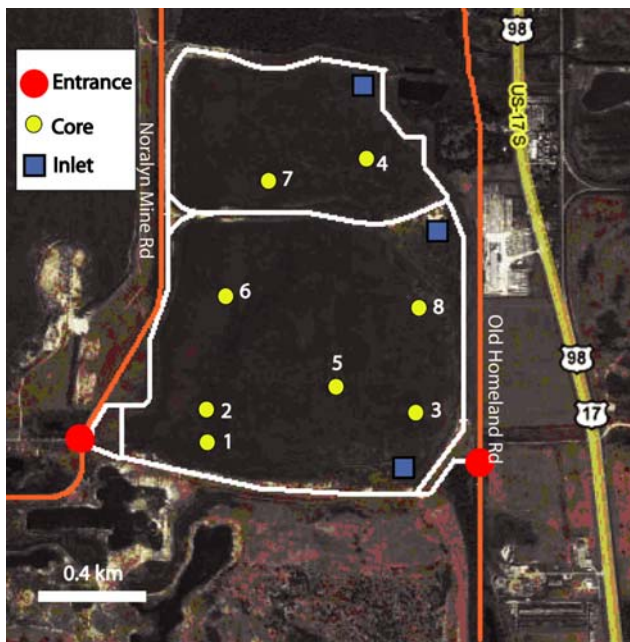


**Fig. 1** Map showing study location. Sites of cores (1–8) are shown along with slurry inlet stations

1.25 m long, 5 cm diameter disposable acetate liners. Immediately following collection, the top and bottom ends of each acetate liner were duct-taped to minimize moisture loss during transport.

Heating methods were used to find bulk moisture content and total organic content. Samples were placed in weighed aluminum dishes and the sample plus dish weight was recorded. Samples were then heated to 120°C for a minimum of 8 h and then reweighed for weight difference. The temperature of 120°C was selected because the corrugated surface of palygorskite crystals holds water more strongly than many other silicate clay minerals (e.g., Jones and Galán 1988). Total organic content was determined by heating at 550°C for 1 h. Grain size investigation was performed by wet sieving material through a 38 µm sieve and comparing mass lost and retained on selected representative samples.

For X-ray Fluorescence (XRF) analysis, samples were dried at 120° C overnight and then powdered for 15 min using a tungsten carbide ball mill. XRF analyses were provided by the Center for Applied Isotope Studies, University of Georgia.

The <2 µm size fraction (upper 5 cm of suspension collected after a 4 h settling time) was collected for all samples and then treated with 3% hydrogen peroxide to remove organic matter by heating each suspension for 4–8 h until no carbon dioxide bubbles were present. This material was then washed four times using deionized water. The clay was exchanged with 0.1 M MgCl<sub>2</sub>· 6H<sub>2</sub>O solution

five times and then washed with deionized water until addition of AgNO<sub>3</sub> solution produced no AgCl. Clay material was removed and smear mounts were prepared on glass slide mounts. X-ray diffraction scans were made using a Panalytical instrument with Cu Kα2 radiation operated at 40 kV and 45 ma. Step size for the scans was 0.03 degrees 2θ with an integrated count time of 20 s per step.

Phyllosilicate minerals were identified using criteria of Moore and Reynolds (1997). Montmorillonite was identified by a broad shaped peak at low angles with a d<sub>(001)</sub> of 1.40–1.65 nm in air dry conditions and a ~1.7 nm peak under ethylene glycol saturated conditions. Selected samples were analyzed using glycerol to confirm the presence of smectite versus vermiculite. Kaolinite was identified by a d<sub>(001)</sub> of approximately 0.715 nm. Palygorskite had non-standard diffraction patterns and was identified using the d<sub>(011)</sub> between 1.02 and 1.08 nm. The standard d<sub>(011)</sub> spacing is 1.04 nm (e.g., Bradley 1940). Illite was identified by a d<sub>(001)</sub> of 1.0 nm. Wavellite was identified by its most intense peak, (020) at approximately 0.86 nm (PDF#25-0020). Apatite was identified using PDF# 09-0432 with d<sub>(211)</sub> = ~0.28 nm, d<sub>(300)</sub> = ~0.27 nm, and d<sub>(202)</sub> = ~0.26 nm. The minor deviation from the ideal standard reflections of (211), (300) and (202) for hydroxyapatite peaks is attributed to the iron and silica content commonly found in these apatites.

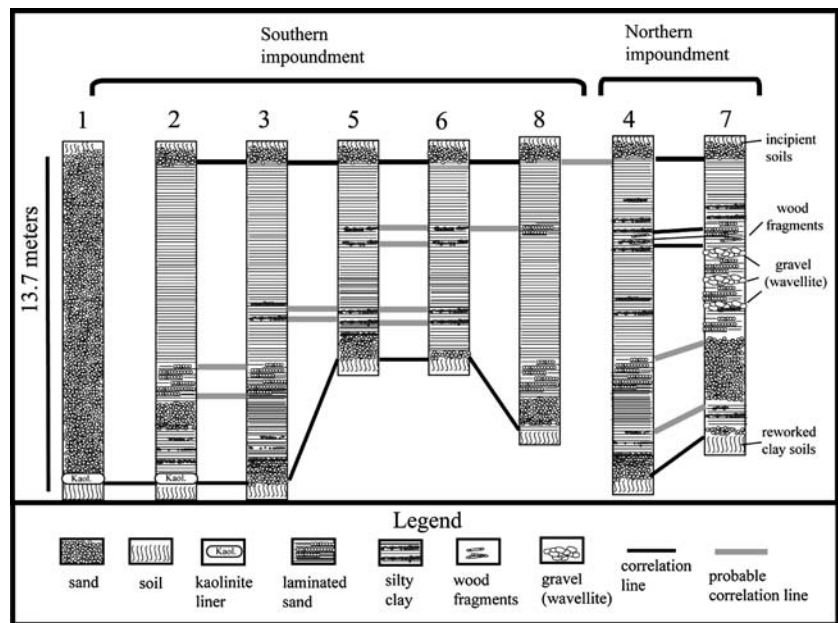
Selected samples were prepared for TEM investigation by taking approximately 1 g and suspending the material in methanol in a small vial for 1 min. A fraction of this was then poured off into a smaller bottle and allowed to settle for 5 min. A drop of this material was then placed on a 3 mm copper grid with a carbon film and allowed to dry for 1 h. TEM analyses were obtained using a 300 kV JEOL JEM-3010 transmission electron microscope equipped with an ultra high-resolution pole piece, resulting in a point to point spatial resolution of 0.17 nm. A 20 µm objective aperture was used for bright field imaging. Images were electronically captured using a Gatan CCD imaging system. Energy dispersive spectra (EDS) were obtained using a Noran EDS system with a 22° take off angle and were done at 400,000 × to ensure no contamination from adjacent particles.

**Results**

Stratigraphy, sedimentology and bulk properties

Stratigraphy of the deposit shows some variability (Fig. 2). Core 1 was placed in the southernmost wall in the southern impoundment. Cores 2,3,5,6 and 8 were placed in clay tailings in the southern impoundment and cores 4 and 7

**Fig. 2** Diagram illustrating the stratigraphy of deposit based on correlation of features in cores. Upper portion of cores is dominated by clay and is referred to as the clay-zone. Note topographic high of pre-existing surface in cores 5 and 6. Probable correlations are based on similar lithology and elevations. A distinct wood fragment zone occurs in cores 4 and 7



were placed in clay tailings in the northern impoundment (Fig. 2). The tops of all the cores 2–8 have 1–2 m of sand with incipient soil features such as animal burrows and spodic iron oxide mottles present. A kaolinite-sand liner approximately 30–40 cm thick was encountered at the bottom of cores 1 and 2. The upper portions of cores 2 and 3 were functionally not recovered in the field owing to drilling operation difficulty but field inspection indicated the material from these cores was clay-rich and visually appears to be the same as equivalent levels in the deposit. Sediment is very clay-rich and is commonly laminated at the millimeter scale with yellow and gray end members. Qualitative comparison with X-ray data suggests yellow sediment has more phosphate minerals while gray sediment has more phyllosilicate minerals. Cores 5 and 6 are shorter than other cores and this is a function of pre-existing topography. Limited stratigraphic markers of wood fragments and organic matter occur in the central portion of cores 4 and 7 in the northern impoundment. Silt-rich layers occur in both impoundments and compose approximately 5–10% of the deposit. Bottom material (generally the lower 1–1.5 m) is a mixture of phosphatic clay and reworked underlying soil material. Sand units are also common in the lower 1–1.5 m. Middle and upper portions of cores 2, 3, 4, 5, 6, and 8 are reasonably homogenous with minor units of organic matter, silt and sand and constitute a clay-rich zone approximately 9.5–7.5 m thick. Core 7 is of interest because it is the most heterogeneous core and has three gravel units in the center and a coarse sand unit present in the bottom of the core. Gravel units are dominated by wavelite with clast sizes 1–3 cm in diameter. Sands from core 7 were also

investigated and were found to be moderate to well rounded and are approximately 85% quartz and 15% apatite. EDS analyses indicate that the apatite in the sand has significant amounts of fluorine, up to 8 weight percent. Gravel clasts are sub-angular to angular and consist solely of wavelite.

Grain size investigation of samples shows that approximately 20% of material in the clay-zone has 50% or more sand. Visual inspection of sands indicates that the mineralogy is dominantly quartz (90%), phosphate grains (5%), oxides and opaque minerals. The remaining samples are silt or clay-rich with 70% of samples having 95% or more material passing the 38  $\mu\text{m}$  sieve.

Both moisture content and total organic content show some variation in the clay zone (Table 1). Moisture content in the clay zone varies from 4.53 to 57.41 wt% and the average percent moisture in the clay zone is approximately 31.0%. There is functionally no correlation of lower water contents with depth and there is also no correlation between moisture content and the abundance of smectite minerals (Fig. 3a). There is functionally no correlation of moisture content with grain size (Fig. 3b). Organic matter occurs largely as deciduous leaves and partially decomposed wood fragments. Organic matter content varies from 0.41 to 9.53% with an average of 3.30%.

#### X-ray fluorescence investigation

Bulk X-ray fluorescence (XRF) investigation (Tables 2, 3) of clay zone samples indicates that the chemical composition of the system is controlled largely by apatite and

**Table 1** Table showing values for bulk properties in percent

Depth (m)	Percent moisture	Percent TOC	Percent solids
<b>Core 2</b>			
7.9	33.79	1.78	64.43
9.3	33.79	1.78	64.43
10.5	27.96	1.71	70.33
<b>Core 3</b>			
6.1	34.04	2.28	63.67
7.6	7.13	0.41	92.46
<b>Core 4</b>			
2.1	35.11	1.91	70.84
3	27.25	2.39	61.26
4.6	36.34	2.95	67.11
6.1	29.94	4.87	59.72
7.6	35.41	4.48	70.66
9.1	24.86	9.53	52.28
11.4	38.19	2.87	97.14
<b>Core 5</b>			
2	29.11	3.65	79.76
3	16.59	3.31	93.28
5.6	3.41	2.32	63.77
6.8	33.91	4.80	43.39
8.2	51.80	6.49	47.86
8.8	45.65	5.91	94.09
<b>Core 6</b>			
2.1	47.39	2.70	49.91
3.7	46.73	4.11	49.16
4.9	55.07	2.61	42.32
6.1	17.60	2.04	80.36
7.3	53.72	2.75	43.53
8.2	33.55	2.90	63.55
<b>Core 7</b>			
1.5	12.16	2.88	84.95
3	12.30	2.29	85.42
4.6	12.30	2.29	85.42
6.7	11.24	2.55	86.20
8.2	49.11	4.56	46.33
10.7	4.53	6.42	89.05
<b>Core 8</b>			
1.5	11.42	3.21	85.36
3	48.53	4.58	46.89
4.6	57.41	3.42	39.17
6.1	43.92	2.20	53.88
7.6	30.84	1.83	67.33
8.5	37.13	2.10	60.77
Average	31.37	3.3	67.11

by the phyllosilicates. The P<sub>2</sub>O<sub>5</sub> concentrations in the samples vary from approximately 4–21 wt%. Comparison of concentrations reveals several relationships. A very

strong correlation ( $r^2 = 0.92$ ) between CaO and P<sub>2</sub>O<sub>5</sub> indicates that apatite is a major control on the phosphate (Fig. 4a). Plots of SiO<sub>2</sub> and P<sub>2</sub>O<sub>5</sub> (Fig. 4b) show a strong correlation ( $r^2 = 0.82$ ) that suggests that the source materials for this particular deposit are comparatively uniform. The strong correlation ( $r^2 = 0.77$ ) of Al<sub>2</sub>O<sub>3</sub> and TiO<sub>2</sub> furthermore suggests that the source materials for this particular clay zone deposit are comparatively uniform and there is a mechanical mixing line of mineral components (Fig. 4c) Qualitatively, two populations seem to be evident based on discrimination of Zr (Fig. 4d).

XRF investigation indicates a number of heavy metal elements and trace elements are common in the samples (Fig. 5). Of particular concern are chromium (0–38 ppm), vanadium (18–492 ppm), nickel (3–129 ppm), zinc (6–193 ppm), lead (8–31 ppm) and copper (0–38 ppm). Cr and V show a strong correlation ( $r^2 = 0.84$ ) as does Cr and Ni ( $r^2 = 0.83$ ) and Cu and Zn ( $r^2 = 0.82$ ). Sr and Pb concentrations exhibit a weak correlation ( $r^2 = 0.56$ ).

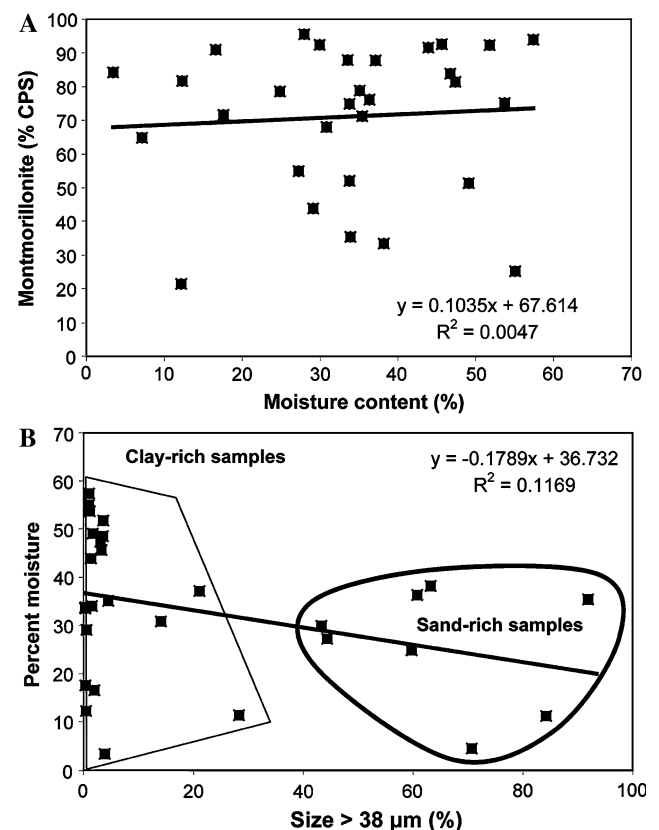


**Fig. 3** a Plot showing percent moisture plotted against abundance of montmorillonite defined as counts per second (cps). There is no correlation between montmorillonite abundance and moisture content. b Plot showing percent moisture plotted against grain size >38 μm. There is functionally no correlation between grain size and particle size. Sand rich samples show nearly as much of a range in moisture content than do clay-rich samples

**Table 2** Concentrations of major elements determined by bulk XRF

Core	Depth (m)	P <sub>2</sub> O <sub>5</sub>	SiO <sub>2</sub>	TiO <sub>2</sub>	Al <sub>2</sub> O <sub>3</sub>	Fe <sub>2</sub> O <sub>3</sub>	MgO	CaO	MnO	Na <sub>2</sub> O	K <sub>2</sub> O	LOI	Totals
1	11.6	4.14	77.85	0.460	12.02	0.60	0.09	0.39	0.004	<0.06	0.14	3.5	99.2
2	7.9	11.24	35.07	0.371	10.17	5.91	5.87	19.12	0.023	0.19	0.52	12.2	100.7
2	9.3	16.18	29.83	0.659	15.44	6.48	3.16	17.25	0.031	0.35	0.57	11.0	100.9
2	10.5	9.88	40.18	0.441	11.40	5.85	5.05	16.30	0.016	0.18	0.51	10.5	100.3
2	11.3	0.42	83.85	0.515	10.96	0.48	0.06	0.14	0.004	<0.06	b.d.	4.4	96.4
2	11.6	0.34	85.41	0.499	10.37	0.43	0.05	0.11	0.004	<0.06	b.d.	2.8	97.2
3	6.1	10.48	36.55	0.539	15.40	6.58	3.32	15.99	0.031	0.18	0.97	10.8	100.8
3	7.6	6.89	74.06	0.342	3.09	1.18	0.30	9.60	0.019	0.21	1.20	3.9	100.8
4	2.1	21.73	26.64	0.432	9.02	2.83	1.47	29.27	0.020	0.24	0.53	7.5	99.7
4	3.0	18.67	32.11	0.401	8.16	2.65	2.07	26.73	0.016	0.33	0.67	8.1	99.9
4	4.6	21.03	35.31	0.343	4.60	1.34	0.95	29.79	0.024	0.33	0.67	6.1	100.5
4	6.1	20.40	35.10	0.392	6.48	1.78	0.94	27.89	0.021	0.26	0.70	6.5	100.5
4	7.6	20.11	39.58	0.340	4.15	1.20	0.52	27.73	0.021	0.25	0.65	6.1	100.7
4	9.1	19.41	37.88	0.370	6.05	1.75	0.88	26.55	0.016	0.23	0.89	5.8	99.8
4	11.4	21.79	31.30	0.394	7.22	1.65	0.89	28.17	0.024	0.29	0.96	8.1	100.8
4	12.2	10.28	64.66	0.367	6.89	3.04	0.24	9.98	0.014	0.22	0.25	4.3	100.2
5	2.0	18.35	25.49	0.479	15.13	4.14	1.56	22.55	0.033	0.29	0.82	11.9	100.7
5	3.0	18.15	26.90	0.478	13.76	4.91	1.62	22.79	0.037	0.23	0.78	10.1	99.8
5	5.6	0.52	83.17	0.509	11.09	0.48	0.07	0.16	0.004	<0.06	0.06	4.9	101.0
5	6.8	18.86	24.81	0.446	14.10	4.17	1.74	24.01	0.034	0.27	0.80	11.0	100.2
5	8.2	14.21	33.78	0.525	14.47	4.27	2.45	19.21	0.028	0.19	0.82	9.8	99.7
5	8.8	14.12	32.00	0.642	16.77	7.44	2.28	16.19	0.029	0.16	0.67	10.4	100.7
6	2.1	16.72	30.58	0.521	12.64	3.53	2.61	22.59	0.014	0.22	0.43	9.3	99.2
6	3.7	21.62	20.78	0.510	12.01	3.40	1.83	29.44	0.025	0.24	0.44	9.1	99.4
6	4.9	21.10	22.64	0.566	14.13	3.46	1.92	26.03	0.023	0.23	0.53	9.8	100.4
6	6.1	15.92	29.31	0.570	13.49	7.42	2.75	20.50	0.039	0.16	0.67	9.3	100.1
6	7.3	18.11	25.54	0.545	15.04	4.72	2.25	23.33	0.025	0.22	0.55	10.4	100.7
7	1.5	4.32	81.93	0.376	6.37	0.80	0.12	2.80	0.005	<0.06	0.22	2.2	99.1
7	3.0	4.45	80.28	0.408	7.43	0.81	0.09	1.90	0.006	<0.06	0.17	5.0	100.5
7	4.6	14.74	32.31	0.544	14.48	5.05	2.81	19.96	0.025	0.17	0.69	9.4	100.2
7	6.7	4.44	80.60	0.373	6.05	1.07	0.11	3.15	0.007	<0.06	0.21	4.2	100.2
7	8.2	18.22	26.30	0.601	16.20	4.21	2.18	21.92	0.022	0.22	0.57	9.4	99.8
7	10.7	7.36	69.87	0.578	13.83	1.29	0.21	0.46	0.006	<0.06	0.36	6.8	100.8
8	1.5	16.06	42.80	0.374	7.05	2.54	1.44	20.91	0.025	0.32	1.01	7.6	100.1
8	3.0	14.62	31.00	0.476	16.91	4.03	1.77	18.86	0.029	0.25	0.92	11.3	100.2
8	4.6	12.70	33.60	0.503	13.97	5.83	3.23	18.60	0.029	0.18	0.80	10.2	99.6
8	6.1	16.40	29.14	0.539	13.69	7.46	2.24	21.17	0.040	0.15	0.71	8.0	99.5
8	7.6	12.72	46.63	0.451	10.16	3.14	1.93	17.88	0.019	0.18	1.00	5.6	99.7
8	8.5	12.14	50.50	0.390	8.58	2.79	1.69	16.81	0.015	0.17	0.86	7.0	100.9

There is no correlation in bulk XRF data with P<sub>2</sub>O<sub>5</sub> content or CaO content with concentrations of Cr and V ( $r^2 = 0.1$  and  $0.12$ , respectively). Comparing ratios of the elements, it becomes clear that the CaO/P<sub>2</sub>O<sub>5</sub> ratio does have a relationship with the V/Cr ratio (Fig. 6). Correlations are moderate with linear regression having  $r^2 = 0.66$

and a natural logarithm regression has an  $r^2 = 0.77$ . Comparing the range of representative CaO/P<sub>2</sub>O<sub>5</sub> ratios reported by Pan and Fleet (2002) suggests that apatite does have some control on the distribution of Cr and V. As for other metals expected to correlate with P<sub>2</sub>O<sub>5</sub> content, Ni and Cu functionally show no correlation with  $r^2 = 0.11$  and

**Table 3** Concentrations of minor elements determined by bulk XRF

Core	Depth (m)	V	Cr	Ni	Cu	Zn	Rb	Sr	Y	Zr	Nb	Ba	La	Ce	Pb	Th
1	11.6	55	122	5	1	11	16	1,075	57	294	9	770	91	146	25	0.3
2	7.9	492	272	129	26	177	39	498	49	96	7	107	27	103	8	3.1
2	9.3	289	282	106	20	162	45	1,371	92	141	13	384	82	145	24	3.8
2	10.5	484	305	123	16	152	38	466	48	109	9	126	31	108	11	3.0
2	11.3	19	82	9	ND	8	11	656	28	424	11	443	98	176	23	ND
2	11.6	18	58	3	ND	6	10	578	27	459	10	450	75	154	23	ND
3	6.1	NA	NA	NA	NA	NA	NA	NA	NA	NA	NA	NA	NA	NA	NA	NA
3	7.6	219	210	74	24	193	36	918	93	215	8	237	45	120	24	2.7
4	2.1	38	21	4	2	20	32	263	42	589	9	324	23	131	12	2.2
4	3.0	303	233	76	16	130	35	950	91	243	7	285	56	129	18	2.5
4	4.6	112	111	38	13	132	32	762	114	384	6	270	65	123	14	2.2
4	6.1	172	170	50	16	133	35	762	105	370	7	286	56	129	21	2.6
4	7.6	123	122	32	11	115	30	651	115	440	6	262	55	126	17	1.9
4	9.1	166	153	38	14	103	38	669	101	341	6	324	66	133	15	2.9
4	11.4	171	169	42	16	126	40	832	114	377	7	353	49	128	15	3.2
4	12.2	81	113	15	3	33	23	739	45	283	9	295	49	126	16	1.1
5	2.0	231	192	32	14	79	59	1,352	96	120	10	505	57	154	31	5.5
5	3.0	234	202	51	15	97	60	1,395	96	128	10	426	71	134	28	5.6
5	5.6	25	51	9	ND	9	11	864	34	423	11	553	129	216	22	b.d.
5	6.8	232	180	36	15	88	57	1,215	101	121	9	513	68	127	28	5.2
5	8.2	NA	NA	NA	NA	NA	NA	NA	NA	NA	NA	NA	NA	NA	NA	NA
5	8.8	NA	NA	NA	NA	NA	NA	NA	NA	NA	NA	NA	NA	NA	NA	NA
6	2.1	357	306	91	38	172	40	1,130	80	102	10	271	57	122	27	3.3
6	3.7	354	294	116	32	193	41	1,465	119	111	9	324	91	136	20	3.3
6	4.9	281	301	92	27	168	46	1,712	138	134	9	534	88	138	25	3.9
6	6.1	449	319	127	20	187	52	892	83	115	11	267	56	129	16	4.7
6	7.3	344	315	110	20	158	46	1,226	88	106	11	376	70	125	22	3.9
7	1.5	41	105	6	1	22	21	663	51	308	8	365	54	134	16	0.9
7	3.0	41	85	7	1	19	17	589	72	354	8	318	50	114	16	0.5
7	4.6	270	271	69	19	155	55	1,008	71	100	11	318	66	128	26	5.1
7	6.7	54	106	7	1	25	20	659	53	341	9	394	64	127	16	0.7
7	8.2	355	333	93	17	150	48	1,369	92	115	12	417	86	140	21	4.2
7	10.7	88	159	6	ND	13	29	1,013	47	273	13	692	93	162	31	1.8
8	1.5	124	117	28	8	66	37	872	85	322	7	433	66	118	20	3
8	3.0	265	211	32	13	79	69	1,083	86	102	10	453	71	123	28	7
8	4.6	283	246	64	16	103	59	784	69	119	11	285	49	148	20	6
8	6.1	413	286	114	23	166	53	918	74	112	11	272	46	129	19	5
8	7.6	343	234	73	16	117	45	570	72	226	9	289	55	112	17	4
8	8.5	280	206	60	14	100	41	549	68	232	8	272	41	117	15	3

0.18, respectively. Sr and Pb also show no correlation with  $P_2O_5$  content, having values of  $r^2 = 0.09$  for Sr and  $r^2 = < 0.00$  for Pb.

#### X-ray diffraction

Powder X-ray diffraction investigation of the  $<2.0 \mu\text{m}$  size fraction of samples indicates that smectite, palygorskite,

kaolinite, illite, apatite and wavellite are common (Table 4). The relative proportions of minerals are variable however smectite (dominantly montmorillonite) is the most abundant phyllosilicate and apatite is the most abundant phosphate mineral. Representative X-ray diffraction patterns are given in Fig. 7.

X-ray diffraction characteristics of phyllosilicates are typical for clays in low temperature sedimentary environments. The  $d_{(001)}$  peaks for smectites have a d-spacing in

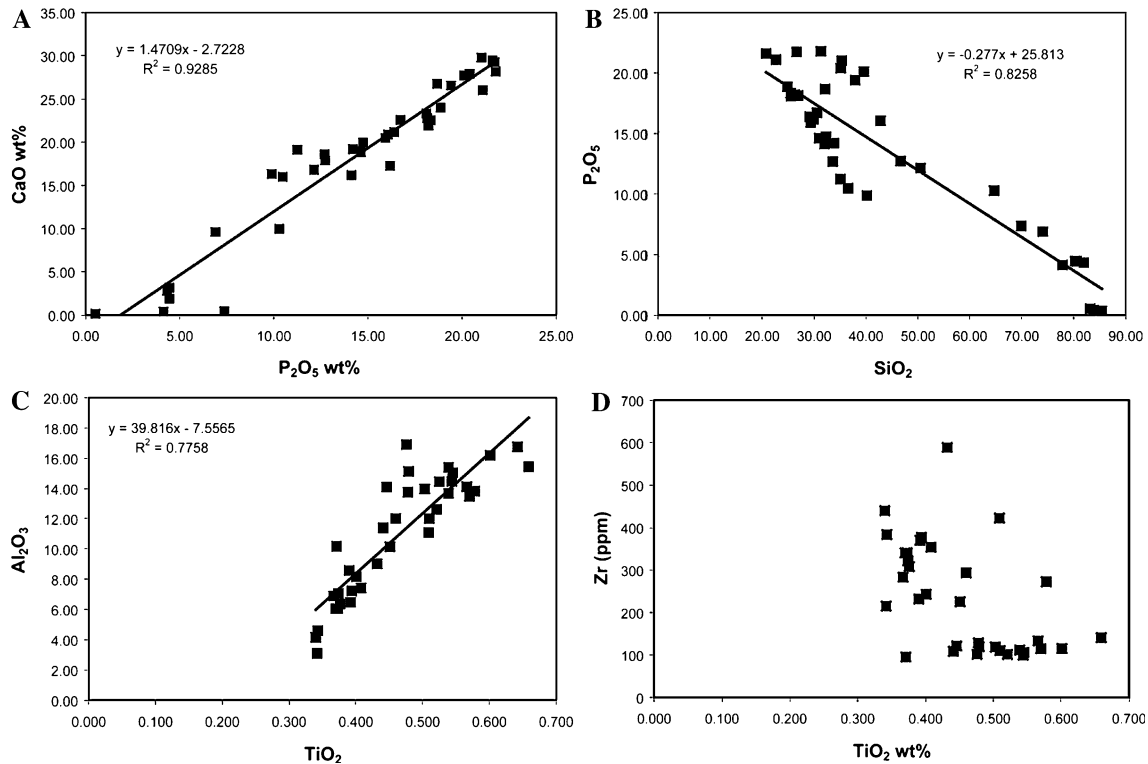


**Fig. 4** Plots of concentrations of major elements determined from XRF. **a** Linear relationship between CaO and P<sub>2</sub>O<sub>5</sub> suggests most of the phosphorous is in apatite. **b** Linear trends in concentrations of P<sub>2</sub>O<sub>5</sub> and SiO<sub>2</sub> suggest mixing of apatite and quartz components. **c**

Plot of Al<sub>2</sub>O<sub>3</sub> and TiO<sub>2</sub> concentrations exhibit a linear relationship. **d** Plots of Zr and TiO<sub>2</sub>. Two populations are apparent based on Zr concentrations above and below approximately 150 ppm

air dry treatment of approximately 1.42 nm and expand in ethylene glycol treatment to a range of approximately 1.69–1.78 nm. Intense (002) peaks were not commonly observed and selected samples investigated under glycerol treatments yielded  $d_{(001)}$  spacings of approximately 1.80 nm indicating that the smectite is dominantly montmorillonite. The  $d_{(001)}$  peaks for illite are approximately 0.98–1.01 nm in all treatments. A broadening of the peak in ethylene glycol treatment is observed in some samples indicating some expandability commonly observed in illites. In heat treatments the  $d_{(001)}$  peaks persist and sharpen. Kaolinite in the clay tailings commonly have  $d_{(001)} = 0.72$ – $0.715$  nm and  $d_{(002)}$  is commonly 0.357–3.50 nm. Kaolinite in the liner samples have similar d-spacings but appear to have sharper peaks. For palygorskite, X-ray diffraction patterns have nonstandard  $d_{(011)}$  spacings that commonly vary from 1.02 to 1.08 nm. The (011) peaks are commonly sharp but other peaks are poorly resolved or of insufficient intensity to be identified.

Limited variation occurs in X-ray diffraction data of phosphate minerals in the clay tailings. Wavellite has  $d_{(020)} = 0.86$  nm which corresponds to (PDF#25-0020). However, wavellite  $d_{(020)}$  can have spacings of 0.84 nm. Apatite

peaks were commonly broad and were identified using PDF# 09-0432 with  $d_{(211)} = \sim 0.28$  nm,  $d_{(300)} = \sim 0.27$  nm, and  $d_{(202)} = \sim 0.26$  nm. The minor deviation from the ideal standard reflections of (211), (300) and (202) for hydroxylapatite peaks is attributed to the iron and silica content commonly found in these apatites and EDS data is presented in the following section.

#### Transmission electron microscopy

Smectite particles are commonly 0.5–1.5  $\mu\text{m}$  in diameter (Fig. 8). Many montmorillonite particles have curled edges, typical of this mineral. Smectite particles commonly occur as irregular foliated lamellar aggregates similar to those described for other smectites by Güven (1988). Selected area electron diffraction patterns of smectites occasionally show discrete spots indicating structural order along (001). The majority of SAED patterns however show rings indicative of turbostratic stacking, commonly observed in smectite (e.g., Güven 1988). The texture and high surface area observed in these particles in part explain the high water contents of the bulk material.



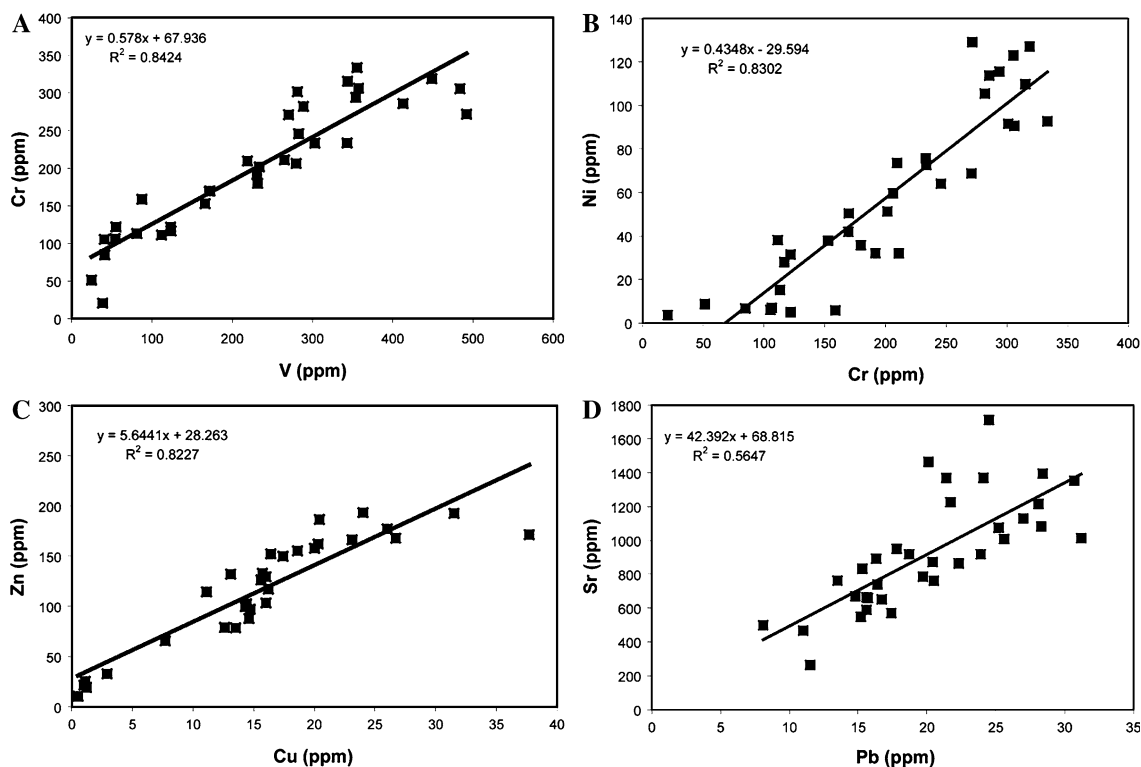


**Fig. 5** Plots showing relationships between concentrations of heavy metals and trace elements in bulk XRF data. Linear relationships with  $r^2 > 0.8$  are observed for **a** Cr and V, **b** Ni and Cr, and **c** Zn and Cu.

A linear relationship exists between Sr and Pb concentrations but with a  $r^2 = 0.56$

EDS analysis on 23 discrete and isolated smectite particles were obtained (Table 5). EDS analysis indicates that the chemical compositions of smectites consists of  $\text{SiO}_2$ ,  $\text{Al}_2\text{O}_3$ ,  $\text{Fe}_2\text{O}_3$ ,  $\text{MgO}$ ,  $\text{CaO}$ ,  $\text{Na}_2\text{O}$ , and  $\text{K}_2\text{O}$ . Chemical compositions are variable and distinct compositions occur. The  $\text{SiO}_2$  content varies from 56.96 to 70.16 wt% with an average of 65.03 wt%.  $\text{Al}_2\text{O}_3$  varies from 11.91 to 29.25 wt% with an average of 16.76 wt%.  $\text{Fe}_2\text{O}_3$  content

varies from 4.78 to 24.85 wt% with an average of 11.00 wt%. concentrations of  $\text{CaO}$  (0.00–2.46 wt%),  $\text{Na}_2\text{O}$  (0.00–0.69 wt%), and  $\text{K}_2\text{O}$  (0.00–0.69 wt%) are consistent with interlayer cations. Overall compositions are consistent with montmorillonite and lesser amounts are consistent with nontronite. Compositions that are intermediate in composition between montmorillonite and nontronite also occur.

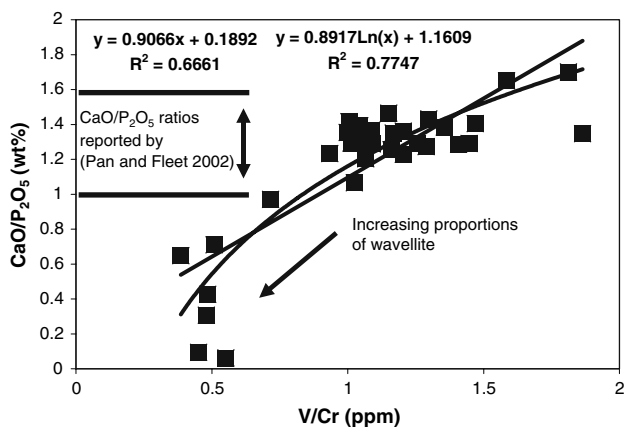


**Fig. 6** Plot showing the distribution of ratios of  $\text{CaO}/\text{P}_2\text{O}_5$  and  $\text{V}/\text{Cr}$  in bulk XRF data. Superimposed for comparison is the range of  $\text{CaO}/\text{P}_2\text{O}_5$  for apatite reported. Most of the bulk XRF data plot in this range

Palygorskite fibers vary in width from approximately 10 to 40 nm, and vary in length from approximately 200 to 1.5  $\mu\text{m}$  (Fig. 9). SAED patterns for palygorskite are heavily streaked along  $[0k0]$ . Chemical components of palygorskite consist of  $\text{SiO}_2$ ,  $\text{Al}_2\text{O}_3$ ,  $\text{Fe}_2\text{O}_3$ ,  $\text{MgO}$ ,  $\text{CaO}$ ,  $\text{Na}_2\text{O}$ , and  $\text{K}_2\text{O}$  (Table 6).  $\text{SiO}_2$  content varies from 67.06 to 75.57 wt%.  $\text{Al}_2\text{O}_3$  content varies from 3.28 to 10.42 wt%.  $\text{Fe}_2\text{O}_3$  has a wide range from 0.80 to 17.64 wt% with an average of 7.05 wt%. A linear relationship ( $r^2 = 0.9255$ ) exists between  $\text{Fe}_2\text{O}_3$  and  $\text{Al}_2\text{O}_3$  content.  $\text{MgO}$  content varies from 10.52 to 15.79 wt%, with an average value of 13.23 wt%. Minor amounts of  $\text{CaO}$ ,  $\text{Na}_2\text{O}$ , and  $\text{K}_2\text{O}$  are observed with values below approximately 0.50 wt%.

Illite occurs as subhedral to anhedral plates and varies in size from approximately 0.1 to 2.0  $\mu\text{m}$  in diameter (Fig. 10). SAED patterns taken along  $[\text{hk}0]$  show well

**Table 4** Summary of abundance of minerals determined by XRD

Core	Depth (m)	Mineral					
		Montmorillonite	Illite	Palygorskite	Kaolinite	Apatite	Wavellite
core 1	11.6 liner	b.d.	b.d.	b.d.	Abundant	b.d.	Trace
core 2	7.9	Abundant	b.d.	Common	Common	Common	Common
core 2	9.3	Abundant	b.d.	Common	Common	Common	Common
core 2	10.5	Abundant	Trace	Common	Common	Common	Common
core 2	11.3 liner	b.d.	b.d.	b.d.	Abundant	b.d.	b.d.
core 2	11.6 liner	b.d.	b.d.	b.d.	Abundant	b.d.	Trace
core 3	6.1	Abundant	b.d.	Common	Common	b.d.	b.d.
core 3	7.6	Abundant	b.d.	Common	Common	Common	b.d.
core 4	2.1	Abundant	b.d.	Common	Common	Common	Common
core 4	3	Abundant	b.d.	Common	Common	Common	Common
core 4	4.6	Abundant	b.d.	Abundant	Common	Abundant	Common
core 4	6.1	Abundant	b.d.	Common	Trace	Common	Common
core 4	7.6	Abundant	b.d.	Common	Common	Common	Common
core 4	9.1	Abundant	b.d.	Common	Trace	Common	Common
core 4	11.4	Abundant	b.d.	Common	Common	Common	Common
core 4	12.2	Abundant	b.d.	Common	Common	Common	Common
core 5	2	Abundant	Common	b.d.	Common	Common	Common
core 5	3	Abundant	Common	Common	Common	Common	b.d.
core 5	5.6	Abundant	Common	Common	Common	Common	Common
core 5	6.8	Abundant	Common	b.d.	Common	Common	Common
core 5	8.2	Abundant	b.d.	b.d.	Common	Common	Common
core 5	8.8	Abundant	b.d.	b.d.	Common	Common	Common
core 6	2.1	Abundant	b.d.	Common	Common	Common	b.d.
core 6	3.7	Abundant	b.d.	Common	Common	Common	b.d.
core 6	4.9	Abundant	Common	b.d.	Common	b.d.	b.d.
core 6	6.1	Abundant		Abundant	b.d.	b.d.	b.d.
core 6	7.3	Abundant	Common	Common	Common	Common	Common
core 7	1.5	Abundant	Common	b.d.	Common	Common	Common
core 7	3	Abundant	Common	b.d.	Common	Common	Common
core 7	4.6	Abundant	Common	b.d.	Common	Common	Common
core 7	6.7	Abundant	Common	b.d.	Common	Common	Common
core 7	8.2	Abundant	b.d.	Common	Common	Common	Common
core 7	10.7	Abundant	Common	b.d.	Common	Common	Common
core 8	1.5	Abundant	Common	b.d.	b.d.	b.d.	b.d.
core 8	3	Abundant	b.d.	b.d.	b.d.	b.d.	b.d.
core 8	4.6	Abundant	Common	Common	Common	Common	Common
core 8	6.1	Abundant	b.d.	Common	Common	Common	Common
core 8	7.6	Abundant	Common	Common	Common	Common	Common
core 8	8.5	Abundant	b.d.	Common	b.d.	Common	Common

b.d. = below detection

defined discrete spots mixed with some rotational streaking, indicating a mixture of highly crystalline material with poorly ordered material. The illite from the clay settling area contains SiO<sub>2</sub>, Al<sub>2</sub>O<sub>3</sub>, Fe<sub>2</sub>O<sub>3</sub>, MgO, CaO, Na<sub>2</sub>O, and K<sub>2</sub>O (Table 7). SiO<sub>2</sub> is most abundant, varying from 54.05

to 62.45 wt%, with an average of 56.72 wt%. Al<sub>2</sub>O<sub>3</sub> ranges from 27.46 to 35.62 wt%, with an average of 31.54 wt%. K<sub>2</sub>O varies from 2.44 to 7.21 wt%. Fe<sub>2</sub>O<sub>3</sub>, content varies from 2.91 to 8.20 wt% and MgO content varies from 0.92 to 3.90 wt%. CaO concentrations are relatively high in

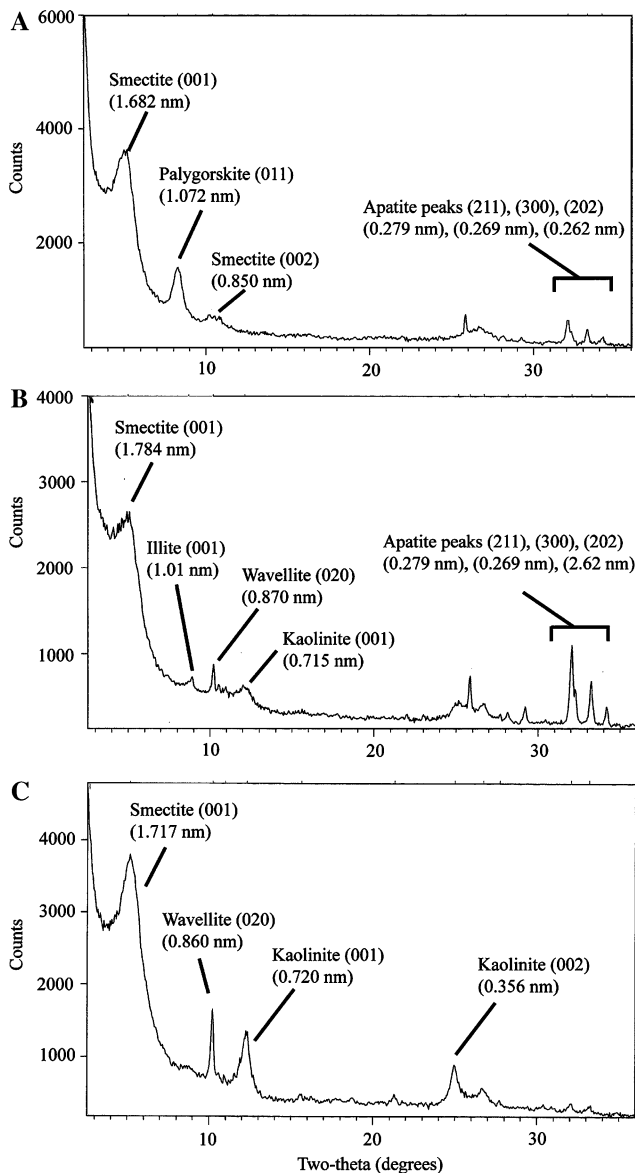


**Fig. 7** Representative X-ray diffraction ethylene glycol saturated patterns of the <2.0  $\mu\text{m}$  size fraction with major peaks labeled. **a** XRD pattern for core 2 at 7.9 m depth showing an example of with abundant palygorskite with a nonstandard d-spacing for (011) of 1.072 nm. A well defined (001) peak smectite is evident as is a low intensity (002) peak. Apatite peaks are labeled on the right. **b** XRD pattern illustrating abundant apatite with peaks labeled on the right. Also present are comparatively broad (001) peaks of illite and kaolinite. The (001) smectite peak is also labeled. **c** XRD pattern showing abundant wavellite and kaolinite. Kaolinite peaks are broad and indicate poor crystallinity

some particles reaching up to 2.29 wt%.  $\text{Na}_2\text{O}$  is present in the low concentrations, with all analyzed samples containing less than 0.50 wt%.

In the <2  $\mu\text{m}$  size fraction phosphate minerals compose approximately 10–40%. Apatite, wavellite and an unidentified Ca–Al–Fe phosphate mineral occur. The unidentified

Ca–Al–Fe phosphate composed 1–5% of the phosphate bearing minerals.

Wavellite occurs discretely as individual grains and less commonly as twins (Fig. 11). Crystals are lath shaped and are commonly 0.1–0.3  $\mu\text{m}$  wide and 0.5–2.0  $\mu\text{m}$  in length. SAED data indicates that the material is highly crystalline. Crystals are also sensitive to beam damage. The chemical composition of wavellite in this deposit consists of  $\text{P}_2\text{O}_5$  and  $\text{Al}_2\text{O}_3$ , with impurities of  $\text{SiO}_2$ ,  $\text{Fe}_2\text{O}_3$ , and  $\text{CaO}$  (Table 8).  $\text{P}_2\text{O}_5$  and  $\text{Al}_2\text{O}_3$  are most abundant with average values of 43.91 and 46.58 wt%, respectively. Concentrations of  $\text{SiO}_2$  have an average of 5.94 wt% and trace amounts of  $\text{Fe}_2\text{O}_3$  and  $\text{CaO}$  are present, with average values of 1.98 and 1.57 wt%, respectively.

Apatite is the most common phosphate mineral composing approximately 80–90% of the total phosphate bearing minerals and approximately 10–45% of the clay fraction. Apatite occurs discretely as individual grains, as twins, or as inter-grown aggregates (Fig. 12). Crystals are commonly euhedral (approximately 85%) to subhedral (approximately 15%) and vary in maximum dimension from approximately 50 to 300 nm. Dimensions of aggregates of apatite grains vary and are commonly between ~0.2 and 2.0  $\mu\text{m}$  in diameter. SAED patterns from discrete apatite crystals all show a very high degree of crystallinity. Complex diffraction patterns from aggregates show discrete spots indicating a high degree of crystallinity.

EDS investigations of apatite were conducted on samples from three cores and some variation in chemical composition was observed (Table 9). Ten discrete crystals of apatite from core 5 were analyzed and the compositions are defined by  $\text{P}_2\text{O}_5$ ,  $\text{SiO}_2$ ,  $\text{Fe}_2\text{O}_3$ , and  $\text{CaO}$ . There is no fluorine, heavy metals, radium or uranium above detection limit (0.10 wt%) within the crystals.  $\text{CaO}$  content has an average value of 54.04 wt% and varies 50.97–57.59 wt%.  $\text{P}_2\text{O}_5$  content has an average 41.90 wt%, and a range of 37.06–46.09 wt%.  $\text{SiO}_2$  and  $\text{Fe}_2\text{O}_3$  are less abundant, with average values of 0.80 and 3.25 wt%, respectively. Twenty discrete apatite crystals from core 6 were investigated and compositions are defined by the components  $\text{P}_2\text{O}_5$ ,  $\text{SiO}_2$ , and  $\text{CaO}$ . There is no fluorine, heavy metals, radium or uranium above detection limit (0.10 wt%) nor is  $\text{Fe}_2\text{O}_3$  present.  $\text{CaO}$  comprises an average of 53.71 wt% and varies from 50.81 to 56.88 wt%.  $\text{P}_2\text{O}_5$  has an average value of 43.32 wt%, with data ranging from 39.08 to 46.17 wt%.  $\text{SiO}_2$  ranges from 0.77 to 8.80 wt% composition, with an average value of 2.96 wt%. Analyses from core 7 show apatite consists of  $\text{P}_2\text{O}_5$ ,  $\text{SiO}_2$ ,  $\text{Fe}_2\text{O}_3$ , and  $\text{CaO}$ .  $\text{P}_2\text{O}_5$  and  $\text{CaO}$  dominate with average values of 43.09 and 54.60 wt%, respectively.  $\text{SiO}_2$  and  $\text{Fe}_2\text{O}_3$  are present with average values of 1.66 and 0.63 wt%. Concentrations for  $\text{CaO}$

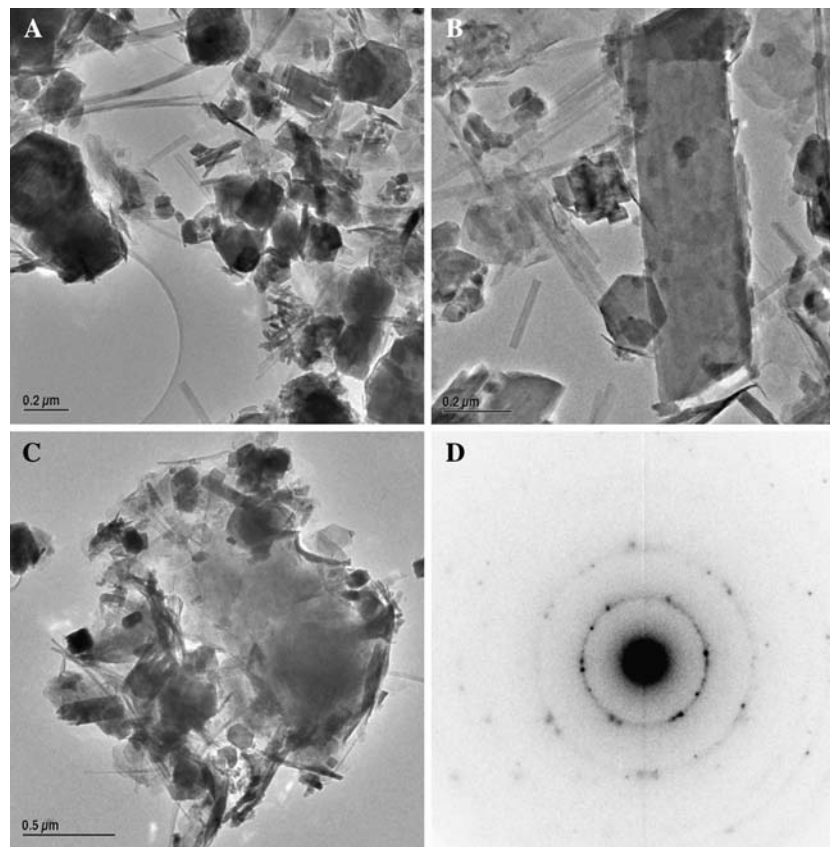


**Fig. 8** **a** TEM image from core 7 at 8.2 m showing an example of the general texture and complexity of the mineral assemblage in the deposit. Blocky crystals are apatite, thin fibers are palygorskite, wide fibers or laths are wavellite and poorly defined platy particles are montmorillonite. **b** TEM image from a sample in core 7 at 8.2 m showing a typical wavellite crystal in the center. Blocky crystals are apatite and smaller fibers are palygorskite. **c** TEM image from core 6 at a depth of 2.1 m showing an aggregate of a montmorillonite particle with palygorskite fibers and apatite crystals, with minor

euhedral crystal of kaolinite. The diameter of the montmorillonite particle is  $\sim 1.5 \mu\text{m}$ . The montmorillonite particle has curled edges, typical of this mineral. Apatite grains are subhedral to euhedral and vary in maximum dimension,  $\sim 0.05$  to  $\sim 0.3 \mu\text{m}$ . Palygorskite fibers are  $\sim 20$  nm wide to  $0.3$ – $0.6 \mu\text{m}$  in length. **d** The SAED pattern is of the montmorillonite particle in the center of C. Discrete spots show some structural order along (001). Rings however show turbostratic stacking, commonly observed in montmorillonite

vary from 39.66 to 60.09 wt% among the samples. There is no fluorine, heavy metals, radium or uranium above detection limit (0.10 wt%) for core 7 samples.

#### Kaolinite liner

The kaolinite liner observed in cores 1 and 2 is approximately 30–40 cm thick and consists of approximately 50% quartz sand and 50% kaolinite. X-ray diffraction patterns of the  $<2.0 \mu\text{m}$  size fraction of the kaolinite liner indicates that it is the only clay mineral present and no secondary phosphate minerals from leakage or mineralization occur (Fig. 13).

Kaolinite crystals occur as subhedral to occasionally euhedral plates  $0.1$ – $1.0 \mu\text{m}$  in diameter. SAED patterns taken along (hk0) of kaolinite show well defined discrete

spots indicating a high degree of crystallinity (Fig. 14). This is typical of kaolinite in the materials studied. EDS data shows limited variation in composition with  $\text{SiO}_2$  varying from 52.08 to 54.94 wt% and  $\text{Al}_2\text{O}_3$  varying from 44.19 to 46.43 wt%. There is appreciable  $\text{Fe}_2\text{O}_3$  content and values range from 0.81 to 1.63 wt%, with an average of 1.23 wt%. TEM investigation indicates that trace quantities ( $<0.01\%$ ) of wavellite occur (Fig. 14).

## Discussion

### Stratigraphy and bulk properties

The stratigraphy of the impoundments represents a continuous fill dominated by clay-sized particles with some silt and sand units. Bottom deposits are more sand and silt rich

**Table 5** EDS analyses of smectite particles

	S1	S2	S3	S4	S5	S6	S7	S8
SiO <sub>2</sub>	60.35	63.25	63.18	68.02	65.88	66.34	64.42	66.19
Al <sub>2</sub> O <sub>3</sub>	29.25	27.14	27.30	13.24	14.48	18.34	18.64	19.53
Fe <sub>2</sub> O <sub>3</sub>	6.22	4.78	4.78	9.60	8.55	6.81	7.55	6.59
MgO	1.67	1.78	1.80	8.15	8.98	7.20	6.48	6.09
CaO	0.26	1.75	2.46	0.99	1.73	0.67	0.80	0.43
Na <sub>2</sub> O	0.69	0.38	0.01	0.00	0.14	0.00	0.42	0.09
K <sub>2</sub> O	1.55	0.93	0.46	0.00	0.24	0.63	1.68	1.08
Total	99.99	100.01	99.99	100.00	100.00	99.99	99.99	100.00
	S9	S10	S11	S12	S13	S14	S15	S16
SiO <sub>2</sub>	64.40	65.12	68.42	69.46	69.68	70.16	69.10	69.54
Al <sub>2</sub> O <sub>3</sub>	18.05	14.25	14.03	11.91	12.42	12.50	13.84	13.88
Fe <sub>2</sub> O <sub>3</sub>	7.67	9.26	7.47	8.63	9.20	8.83	9.84	9.88
MgO	7.06	9.43	9.07	9.12	7.79	7.41	6.06	5.83
CaO	0.69	0.58	0.65	0.88	0.90	1.03	1.15	0.87
Na <sub>2</sub> O	0.00	0.00	0.00	0.00	0.00	0.00	0.00	0.00
K <sub>2</sub> O	2.12	1.35	0.36	0.00	0.00	0.08	0.00	0.00
Total	99.99	99.99	100.00	100.00	99.99	100.01	99.99	100.00
	S17	S18	S19	S20	S21	S22	S23	
SiO <sub>2</sub>	67.16	67.62	67.86	57.28	56.96	57.93	57.32	
Al <sub>2</sub> O <sub>3</sub>	18.12	18.05	17.77	13.00	13.56	12.43	13.69	
Fe <sub>2</sub> O <sub>3</sub>	9.79	9.70	9.66	24.21	24.85	24.51	24.57	
MgO	3.62	3.60	3.70	3.91	3.37	3.43	3.33	
CaO	1.18	1.01	0.99	1.47	1.08	1.45	1.01	
Na <sub>2</sub> O	0.00	0.00	0.00	0.00	0.10	0.17	0.02	
K <sub>2</sub> O	0.12	0.01	0.01	0.12	0.09	0.09	0.08	
Total	99.99	99.99	99.99	99.99	100.01	100.01	100.02	

but the upper 7.5–9.5 m of the tailings deposit are dominated by clay. Laminations in the clay are well developed and there is no indication of reworking of the sediment in the clay zone. The exception to this is the three coarse-grained layers in core 7.

Coarse grained material in core 7 is interpreted as debris flow from impoundment wall materials because of its proximity (approximately 65 m) to the southern wall of the northern impoundment. The layers may also reflect dump material that was not suitable for processing into finished phosphate product. The core is placed far from input sites and as the gravel units are not graded with respect to grain size they do not reflect hydraulic surges of input. Both interpretations for the cause of the coarse units are viable. Impoundment wall failures occurred in other clay tailing sites in the 1940s–1970s (LaFevers et al. 1977) and the coarse grained units may reflect similar but smaller scale processes. Coarse grained units are not expected in clay

tailings and these units likely cause local variation and increases in permeability coefficients.

Both organic matter content and bulk moisture content exhibit variation. Organic matter content was variable and no clear trend with depth could be identified, however higher organic contents were observed in some samples at depth. These higher organic matter contents are related to diffuse wood particles. The large variation in moisture content in the clay zone is a function of multiple processes that include dewatering, evaporation and molecular water sorbed to minerals. The occurrence of some low (~4 to 7 wt%) water contents observed at depth and some comparatively high (>50%) water contents observed in the middle level of the unit suggests that some mechanical dewatering has occurred. Moisture content does not clearly follow mineral composition or grain size. Specifically there is no correlation with the abundance of montmorillonite and this is unexpected. Montmorillonite has long been

**Fig. 9** TEM images of palygorskite. **a** TEM image of sample from core 7 at 8.2 m showing a bundle of palygorskite fibers. Fibers are commonly 10–20 nm wide and are intimately inter-grown. **b** A bundle of palygorskite fibers from core 6 at 2.1 m. Fibers vary in width between approximately 10–20 nm. This texture is very representative of palygorskite fibers in the deposit. **c** TEM image from core 7 at 8.2 m showing aggregate of apatite crystals left center with a discrete palygorskite fiber in the upper center portion of the image. **d** SAED pattern of the palygorskite fiber in D the previous image showing strong streaking along (hk0). Such streaking in diffraction patterns is common in palygorskite

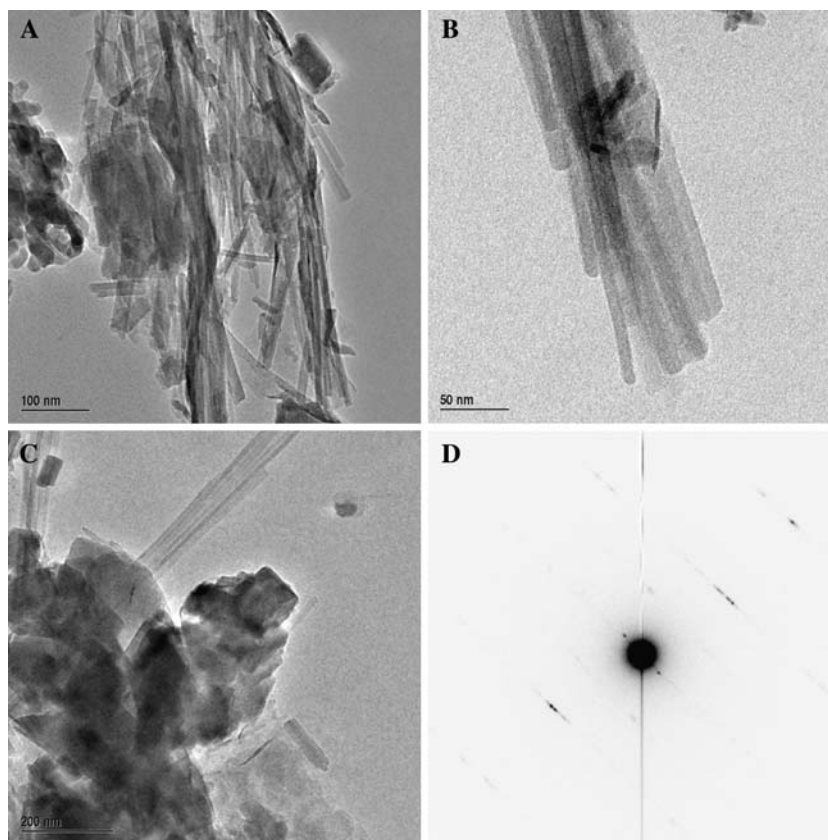


**Table 6** EDS analyses of palygorskite particles

	P1	P2	P3	P4	P5
SiO <sub>2</sub>	75.57	74.80	70.02	74.70	69.99
Al <sub>2</sub> O <sub>3</sub>	6.52	5.82	6.62	5.81	6.61
Fe <sub>2</sub> O <sub>3</sub>	6.88	7.76	6.99	7.75	6.99
MgO	10.52	10.85	15.79	10.84	15.78
CaO	0.51	0.39	0.58	0.39	0.58
Na <sub>2</sub> O	0.00	0.37	0.00	0.37	0.00
K <sub>2</sub> O	0.00	0.00	0.00	0.14	0.04
Total	100.00	99.99	100.00	100.00	99.99
	P6	P7	P8	P9	P10
SiO <sub>2</sub>	74.33	73.79	74.82	67.06	69.58
Al <sub>2</sub> O <sub>3</sub>	10.42	8.68	9.20	3.28	4.66
Fe <sub>2</sub> O <sub>3</sub>	0.80	2.91	1.32	17.64	11.51
MgO	14.28	14.07	14.66	11.27	14.25
CaO	0.00	0.00	0.00	0.00	0.00
Na <sub>2</sub> O	0.00	0.00	0.00	0.23	0.00
K <sub>2</sub> O	0.18	0.56	0.00	0.51	0.00
Total	100.01	100.01	100.00	99.99	100.00

recognized to be able to absorb large amounts of water and under ideal conditions can expand such that  $d_{(001)} = 14.0$  nm (Norrish 1954). The variation in moisture content

remains problematic and detailed explanations for this variation are not posed here. It is clear however that simple dewatering models or models based on mineralogical variation are inadequate to describe the variability and further investigations need to be made.

#### XRF

The chemical composition of bulk sediment is a function of mineralogy and mixing of minerals through sedimentological processes plays a primary role in controlling the bulk chemical composition. Variation in bulk chemical composition in turn is a function of variation of mineral content.

For hydroxyapatite the ideal CaO/P<sub>2</sub>O<sub>5</sub> ratio is 1.31 which should approximate the slope of the regression line for the pure case. The deviation from the ideal in the bulk XRF data can be explained by the occurrence of wavellite (aluminum phosphate) which has little or no CaO component and minor amounts of complex phosphate minerals which may have higher contents. Furthermore the deviation can be explained by an average concentration of 1.23 wt% CaO in smectite particle.

Bulk XRF data show linear correlations suggesting a single source type of materials with variable abundances of

**Fig. 10** **a** TEM image of illite particle showing straight lattice fringes. The particle is adhered to a smectite particle. **b** SAED of illite particle with characteristic streaking indicating stacking disorder typical for this mineral

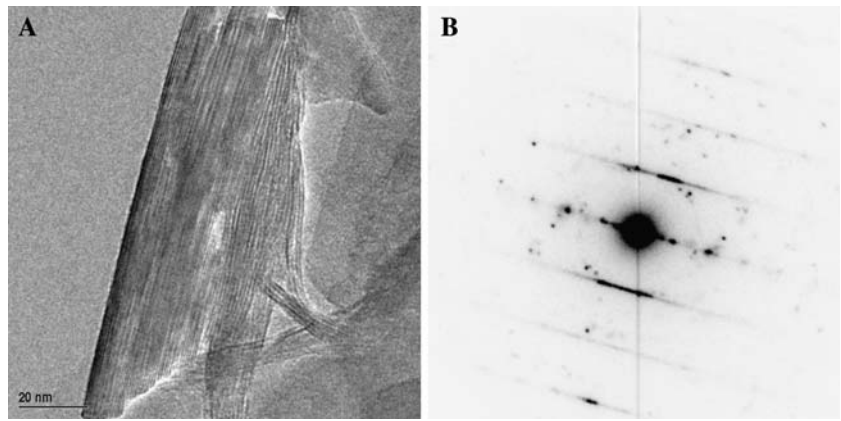


**Table 7** EDS analyses of illite particles

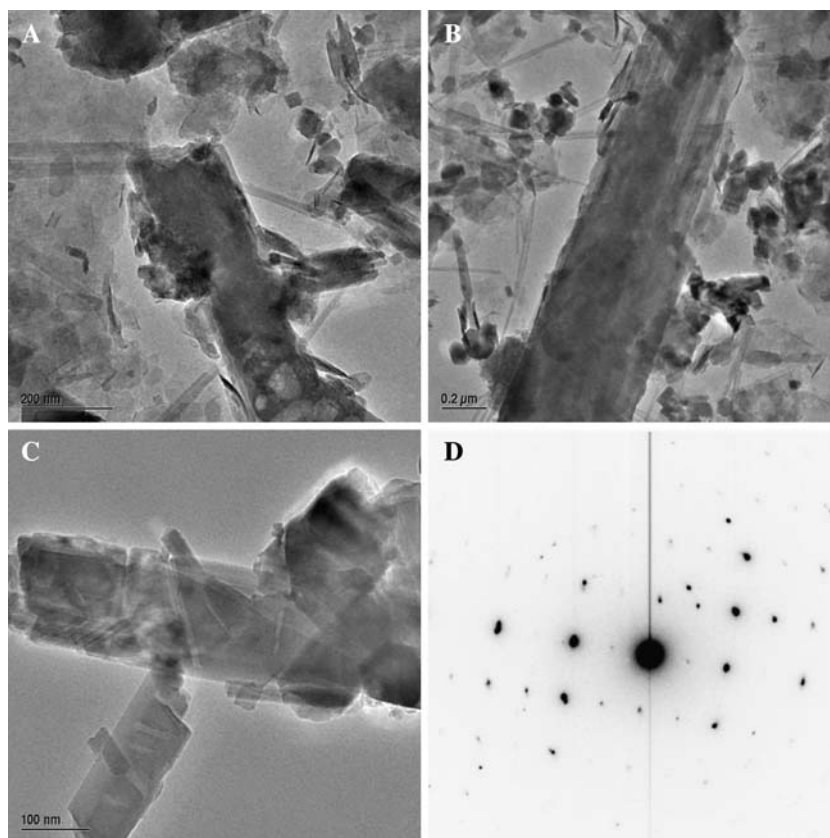
	I1	I2	I3	I4	I5	I6	I7
SiO <sub>2</sub>	62.45	57.19	54.05	55.37	55.72	56.90	56.30
Al <sub>2</sub> O <sub>3</sub>	27.46	30.33	31.55	30.83	30.16	30.05	31.35
Fe <sub>2</sub> O <sub>3</sub>	5.06	3.97	8.16	8.20	7.07	4.37	6.08
MgO	1.85	1.76	2.65	1.74	1.99	3.33	2.10
CaO	0.09	2.29	0.75	1.15	0.00	0.00	0.00
Na <sub>2</sub> O	0.43	0.37	0.40	0.00	0.00	0.00	0.00
K <sub>2</sub> O	2.67	4.09	2.44	2.71	5.07	5.35	4.16
Total	100.01	100.00	100.00	100.00	100.01	100.00	99.99
	I8	I9	I10	I11	I12	I13	I14
SiO <sub>2</sub>	57.94	60.52	57.83	57.31	57.93	57.32	55.85
Al <sub>2</sub> O <sub>3</sub>	30.08	29.61	30.90	33.54	31.48	29.28	31.09
Fe <sub>2</sub> O <sub>3</sub>	4.99	4.73	3.91	3.09	3.94	5.15	4.42
MgO	2.38	2.57	2.91	2.53	3.42	3.90	1.31
CaO	0.00	0.00	0.00	0.00	0.00	0.00	0.00
Na <sub>2</sub> O	0.00	0.00	0.00	0.00	0.00	0.00	0.12
K <sub>2</sub> O	4.61	2.58	4.45	3.52	3.23	4.34	7.21
Total	100.00	100.01	100.00	99.99	100.00	99.99	100.00
	I15	I16	I17	I18	I19	I20	I21
SiO <sub>2</sub>	56.17	55.16	56.50	54.25	54.73	55.79	55.93
Al <sub>2</sub> O <sub>3</sub>	30.86	33.04	32.84	33.73	34.37	34.14	35.62
Fe <sub>2</sub> O <sub>3</sub>	4.74	4.27	4.32	3.83	3.60	3.25	2.91
MgO	2.22	1.69	1.64	1.44	1.40	1.47	0.92
CaO	0.00	0.00	0.00	0.00	0.00	0.00	0.00
Na <sub>2</sub> O	0.12	0.08	0.00	0.00	0.14	0.00	0.00
K <sub>2</sub> O	5.90	5.76	4.70	6.75	5.75	5.35	4.61
Total	100.01	100.00	100.00	100.00	99.99	100.00	99.99

minerals. Ratios for certain components are reasonably uniform however the concentrations of these components can vary greatly and the variation is interpreted to reflect mechanical mixing of differing proportions of minerals. The plot of SiO<sub>2</sub> and P<sub>2</sub>O<sub>5</sub> show a correlation ( $r^2 = 0.82$ )

however, there is a deviation of some samples and this is interpreted as mechanical mixing line with relative increases in wavellite (aluminum phosphate).

Both Zr and Ti are elements that are commonly considered to be chemically immobile and thus can be a

**Fig. 11** TEM images of wavellite particles. **a** Center particle shows an example of a moderately tabular wavellite crystal with rounded termination and overgrowths of apatite on the left edge. **b** Euhedral crystal comparatively free of overgrowths. **c** Intergrowth of euhedral wavellite crystals with no overgrowths. **d** SAED pattern from the left portion of the large crystal in C



fingerprint for source materials. The two populations of analyses based on discrimination of zirconium is likely a function of hydrodynamics of the deposit. Zr is almost exclusively found in zircon in sedimentary environments and zircon is a heavy mineral ( $D = 4.67$ ). The variation in abundance of bulk Zr likely is a sedimentological phenomenon with higher concentrations of Zr associated with deposition of more zircon at lower flow velocities. Similarly titanium is found in  $\text{TiO}_2$  polymorphs, commonly rutile, and is also a heavy mineral ( $D = 4.25$ ). Both Zr and Ti concentrations are not high enough to be economically viable for mining and the grain size is prohibitory for mechanical separation.

### Mineralogy

Phyllosilicates compose an estimated 55–85% of the tailings. The phyllosilicate mineralogy of the deposit is dominated by smectite (largely montmorillonite), palygorskite, with far lesser amounts of illite and kaolinite. Although there is variability between cores no systematic spatial variation in the relative proportions of phyllosilicates was observed in the clay deposit. Energy dispersive spectroscopy EDS analysis indicates that chemical compositions of phyllosilicates are somewhat typical but

overall are enriched with respect to Fe compared to theoretical end members. The relative enrichment of Fe is interpreted to be a primary sedimentary feature and not the result of treatment owing to mine processing. The high percentages of montmorillonite and palygorskite in part explain the high bulk water contents observed.

Smectite particles occur primarily as irregular foliated lamellar aggregates and have variable chemical composition. Most particles analyzed are montmorillonite and particles have an average of approximately 11.00 wt%  $\text{Fe}_2\text{O}_3$ . This composition is consistent with solid solution with nontronite. Some compositions are consistent with near end member nontronite. Chemical composition of particles indicate they may be R0 illite–montmorillonite because their  $\text{K}_2\text{O}$  content is approximately 1–2 wt%. The mixed assemblage of smectite minerals prevents a definitive X-ray diffraction identification of R0 illite–smectite owing to peak overlap of the  $d_{(001)}$  peak in ethylene glycol treatment. Multiple chemical compositions of smectite have not previously been recognized in these deposits and these compositions illustrate the complexity of the mineralogy. Smectites likely were of both detrital and authigenic origin in the ore material. Krekeler et al. (2004) and Krekeler (2004) showed that both detrital and authigenic montmorillonites are common in the broadly related palygorskite-rich clays of the Hawthorne Formation in southern Georgia.



**Table 8** EDS analyses of wavellite particles

Wavellite	W1	W2	W3	W4	W5	W6	W7
P <sub>2</sub> O <sub>5</sub>	44.85	44.03	43.54	41.27	45.70	46.97	47.18
SiO <sub>2</sub>	6.28	6.89	6.07	10.23	4.99	2.78	2.90
Al <sub>2</sub> O <sub>3</sub>	46.66	46.84	48.13	44.87	45.97	46.94	46.52
Fe <sub>2</sub> O <sub>3</sub>	1.82	1.46	1.29	1.87	1.53	1.90	2.25
MgO	0.00	0.00	0.00	0.00	0.00	0.00	0.00
CaO	0.39	0.77	0.97	1.77	1.81	1.42	1.14
Na <sub>2</sub> O	0.00	0.00	0.00	0.00	0.00	0.00	0.00
K <sub>2</sub> O	0.00	0.00	0.00	0.00	0.00	0.00	0.00
F	0.00	0.00	0.00	0.00	0.00	0.00	0.00
Sum	100.00	99.99	100.00	100.01	100.00	100.01	99.99
	W8	W9	W10	W11	W12	W13	W14
P <sub>2</sub> O <sub>5</sub>	40.89	43.91	43.52	42.26	44.77	42.26	43.63
SiO <sub>2</sub>	4.11	3.33	7.13	7.74	5.55	7.74	7.49
Al <sub>2</sub> O <sub>3</sub>	50.18	47.00	45.10	45.48	47.42	45.48	45.50
Fe <sub>2</sub> O <sub>3</sub>	1.66	2.19	2.55	2.75	1.74	2.75	1.99
MgO	0.00	0.00	0.00	0.00	0.00	0.00	0.00
CaO	3.15	3.56	1.70	1.76	0.52	1.76	1.39
Na <sub>2</sub> O	0.00	0.00	0.00	0.00	0.00	0.00	0.00
K <sub>2</sub> O	0.00	0.00	0.00	0.00	0.00	0.00	0.00
F	0.00	0.00	0.00	0.00	0.00	0.00	0.00
Sum	99.99	99.99	100.00	99.99	100.00	99.99	100.00

The morphology of palygorskite fibers are overall very similar to other palygorskite fibers found in the Hawthorne Formation in southern Georgia (Krekeler 2004; Krekeler et al. 2004, 2005). Palygorskite fibers have Fe<sub>2</sub>O<sub>3</sub> contents up to 17.64 wt%. This is comparatively high with respect to other Hawthorne Formation palygorskites which typically vary from 3 to 7 wt% Fe<sub>2</sub>O<sub>3</sub> (Krekeler 2004; Krekeler et al. 2004, 2005) and with palygorskites considered Fe-rich such as Gr-1 investigated by Gionis et al. (2006). The linear relationship observed between Al<sub>2</sub>O<sub>3</sub> and Fe<sub>2</sub>O<sub>3</sub> content is interpreted as solid solution in the octahedral sites. Güven et al. (1992) used NMR spectroscopy techniques to investigate the nature of coordination of aluminum sites in the PFL-1 palygorskite and determined that only Si occurred in tetrahedral sites and Al<sup>3+</sup> and Fe<sup>3+</sup> occurs in the octahedral sites.

SAED patterns of all of the palygorskite fibers show strong streaking along (hk0). This indicates that there is much structural disorder in the fibers and is interpreted as variations in defects and polysome width. Krekeler and Guggenheim (2007) have shown a variety of defects to occur in palygorskite–sepiolite minerals including stacking disorder, polysome width variation and open channel defects. The occurrence of defects in palygorskite in the deposit of the present study explains why X-ray diffraction patterns have nonstandard d<sub>(011)</sub> spacings that commonly

vary from 1.02 to 10.8 nm. The d<sub>(011)</sub> spacing for palygorskite is 1.04 nm (Bradley 1940). Larger d<sub>(011)</sub> spacings may be the result of larger polysome width and Fe substitution in octahedral sites as the radius of Fe<sup>3+</sup> in silicates is approximately 0.067 nm and Al<sup>3+</sup> is approximately 0.057 nm (e.g., Bloss 1997).

Illite is a minor phyllosilicate and is a primary control on the distribution of potassium. The morphology of illite particles are platy and the subhedral morphology is consistent with a detrital origin in the original ore material. Overall the chemical compositions are consistent with common illites observed in shales and sedimentary rocks (e.g., Srodon 1984). Illite has an affinity for the adsorption of some heavy metals (e.g., Gu and Evans 2007) however these interactions are surface related and illite likely plays a minor role on the distribution of heavy metals in the deposit.

Vanadium and chromium can substitute in apatites (Pan and Fleet 2002; Dai and Hughes 1989; Sudarsanan et al. 1977; Banks et al. 1971; Banks and Jaunarajs 1965). However, there is functionally no correlation in bulk XRF data with P<sub>2</sub>O<sub>5</sub> content or CaO content with concentrations of Cr (*r*<sup>2</sup> = 0.10–0.12) and no V or Cr was observed in any of the EDS analysis of individual grains or crystals of apatite. Yet in comparing ratios it becomes clear that the bulk XRF CaO/ P<sub>2</sub>O<sub>5</sub> ratio does have a relationship with

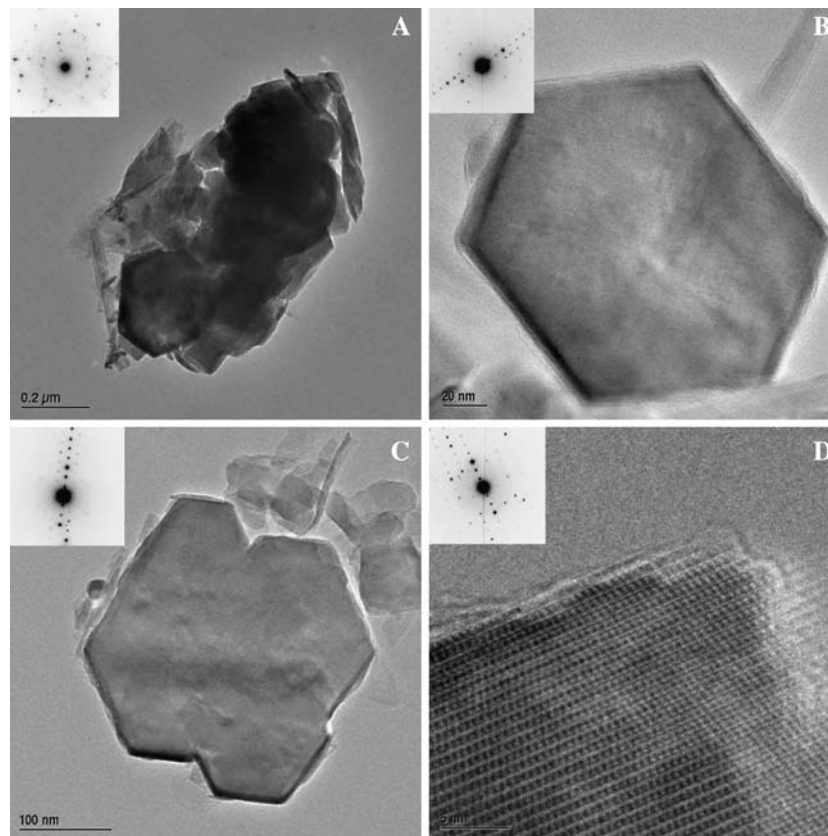


**Fig. 12** TEM images with SAED patterns showing representative textures of apatite. **a** The center portion of the image shows large aggregates of apatite grains with phyllosilicates adhering to the surface. The sample is from core 6 at a depth of 2.1 m. Grains are euhedral to subhedral with dimensions that vary  $\sim 0.2$  to  $0.5 \mu\text{m}$ . Grains are inter-grown in a randomly oriented texture. **b** Example of a euhedral, uniform apatite crystal viewed along the *c*-axis from core 2 at a depth of 7.9 m. The crystal is approximately 140 nm in diameter and is typical of individual crystals of apatite observed. The

SAED pattern shows the particle to be a single crystal. **c** Example of a euhedral twinned apatite crystal from core 7 at a depth of 8.2 m. The crystal is approximately 350 nm in diameter and is typical of twinned individual crystals of apatite observed. The SAED pattern is coherent and shows the particle to be a single crystal with no misalignment along the *c*-axis. **d** A structural image showing lattice fringes of an individual crystal from core 2 at a depth of 11.6 m. The SAED pattern shows the particle to be a single crystal

the bulk XRF V/Cr ratio suggesting that apatite does have some control on the distribution of Cr and V. Moderate correlations exist with linear regressions having  $r^2 = 0.66$  and a natural logarithm have  $r^2 = 0.77$  and the lack of a stronger correlation may be explained by a number of factors. V and Cr form solid solution with a number of low temperature phosphate minerals and this may explain some of the poor correlation. Alternatively, oxides such as hematite can have trace and minor quantities of Cr and V. For hematite there is solid solution between eskolaite  $\text{Cr}_2\text{O}_3$  and karelianite  $\text{V}_2\text{O}_3$ . Trace, minor and even major quantities of these metals can occur in spinel minerals. For example, Cr forms solid solution with magnetite and is a major constituent of chromite. Similarly vanadium occurs in magnetite at minor concentrations and is a major constituent of coulsonite. Trace amounts of magnetite grains and opaques were observed in selected sand samples and this may explain some of the variation observed.

The correlation of concentrations of Sr and Pb suggests that these elements may be in a single mineral phase and there is ample literature describing the substitution of  $\text{Sr}^{2+}$  and  $\text{Pb}^{2+}$  in the apatite structure (Khattech and Jamel 1997; Hughes et al. 1991; Verbeck et al. 1981; Heijligers et al. 1979; Engel et al. 1975; Kreidler and Hummel 1970; Akhavan-Niaki 1961). However there is no correlation between ratios or concentrations of Sr, Pb, CaO and  $\text{P}_2\text{O}_5$  in the bulk XRF data. Sr and Pb show no correlation with  $\text{P}_2\text{O}_5$  content having values of  $r^2 = 0.09$  for Sr and  $r^2 = 0.00$  for Pb. This lack of correlation is unexpected owing to the strong affinity of Sr and Pb for phosphate minerals and suggests that multiple minerals contain Sr and Pb. These cations may be in interlayer sites of smectite minerals and zeolite-like channels of palygorskite.

The EDS analyses on apatite in the indicated that fluorine is below detection limits in clay sized material but is present in sand-sized grains. Fe and Si are also common in

**Table 9** EDS analyses of apatites

	A 5-1	A 5-2	A 5-3	A 5-4	A 5-5	A 5-6	A 5-7	A 5-8
P <sub>2</sub> O <sub>5</sub>	46.09	41.95	40.08	38.12	37.06	43.88	44.56	42.69
SiO <sub>2</sub>	0.53	0.45	0.52	0.04	0.19	2.01	0.88	0.90
Fe <sub>2</sub> O <sub>3</sub>	2.40	2.39	4.42	5.32	5.15	1.37	0.89	3.70
CaO	50.97	55.22	54.98	56.53	57.59	52.75	53.67	52.71
F	0.00	0.00	0.00	0.00	0.00	0.00	0.00	0.00
Total	99.99	100.01	100.00	100.01	99.99	100.01	100.00	100.00
	A 5-9	A 5-10	A 6-1	A 6-2	A 6-3	A 6-4	A 6-5	A 6-6
P <sub>2</sub> O <sub>5</sub>	42.30	42.32	43.37	42.19	44.12	43.46	46.17	39.08
SiO <sub>2</sub>	0.98	1.52	2.26	1.29	2.57	2.49	1.54	7.51
Fe <sub>2</sub> O <sub>3</sub>	3.93	2.93	0.00	0.00	0.00	0.00	0.00	0.00
CaO	52.79	53.23	54.38	56.52	53.31	54.05	52.29	53.40
F	0.00	0.00	0.00	0.00	0.00	0.00	0.00	0.00
Total	100.00	100.00	100.01	100.00	100.00	100.00	100.00	99.99
	A 6-7	A 6-8	A 6-9	A 6-10	A 6-11	A 6-12	A 6-13	A 6-14
P <sub>2</sub> O <sub>5</sub>	40.93	40.39	44.25	44.78	43.84	45.07	41.81	42.44
SiO <sub>2</sub>	5.69	8.80	3.19	2.28	3.07	3.42	1.32	1.33
Fe <sub>2</sub> O <sub>3</sub>	0.00	0.00	0.00	0.00	0.00	0.00	0.00	0.00
CaO	53.38	50.81	52.55	52.94	53.09	51.51	56.88	56.23
F	0.00	0.00	0.00	0.00	0.00	0.00	0.00	0.00
Total	100.00	100.00	99.99	100.00	100.00	100.00	100.01	100.00
	A 6-15	A 6-16	A 6-17	A 6-18	A 6-19	A 6-20	A 7-1	A 7-2
P <sub>2</sub> O <sub>5</sub>	43.08	43.87	42.55	45.11	44.76	45.22	43.75	43.66
SiO <sub>2</sub>	0.77	4.66	3.13	1.13	0.96	1.82	1.55	1.55
Fe <sub>2</sub> O <sub>3</sub>	0.00	0.00	0.00	0.00	0.00	0.00	0.50	0.51
CaO	56.16	51.46	54.32	53.76	54.28	52.96	54.20	54.29
F	0.00	0.00	0.00	0.00	0.00	0.00	0.00	0.00
Total	100.01	99.99	100.00	100.00	100.00	100.00	100.00	100.01
	A 7-3	A 7-4	A 7-5	A 7-6	A 7-7	A 7-8	A 7-9	A 7-10
P <sub>2</sub> O <sub>5</sub>	44.01	41.21	42.02	42.86	43.87	44.72	43.69	44.05
SiO <sub>2</sub>	1.39	1.65	2.23	2.52	1.59	1.01	1.62	0.98
Fe <sub>2</sub> O <sub>3</sub>	0.52	0.53	0.41	0.40	0.46	0.67	0.92	0.43
CaO	54.09	56.61	55.34	54.22	54.08	53.60	53.77	54.53
F	0.00	0.00	0.00	0.00	0.00	0.00	0.00	0.00
Total	100.01	100.00	100.00	100.00	100.00	100.00	100.00	99.99
	A 7-11	A 7-12	A 7-13	A 7-14	A 7-15	A 7-16	A 7-17	A 7-18
P <sub>2</sub> O <sub>5</sub>	57.40	47.01	41.34	41.78	37.66	41.34	42.02	42.08
SiO <sub>2</sub>	2.47	1.20	2.04	1.27	1.62	2.04	1.58	1.13
Fe <sub>2</sub> O <sub>3</sub>	0.48	0.43	0.77	0.65	0.63	0.77	0.81	1.03
CaO	39.66	51.36	55.85	56.30	60.09	55.85	55.59	55.76
F	0.00	0.00	0.00	0.00	0.00	0.00	0.00	0.00
Total	100.01	100.00	100.00	100.00	100.00	100.00	100.00	100.00

**Table 9** continued

	A 7-19	A 7-20	A 7-21	A 7-22	A 7-23
P <sub>2</sub> O <sub>5</sub>	42.02	41.29	40.60	39.81	43.02
SiO <sub>2</sub>	0.91	0.90	2.47	3.32	1.16
Fe <sub>2</sub> O <sub>3</sub>	0.66	0.42	0.89	1.37	0.38
CaO	56.40	57.39	56.04	55.50	55.44
F	0.00	0.00	0.00	0.00	0.00
Total	99.99	100.00	100.00	100.00	100.00

the clay size fraction apatite. Apatites do not commonly have much Fe content and usually Fe is in trace quantities (Pan and Fleet 2002). The Fe<sub>2</sub>O<sub>3</sub> content of apatite in the clay fractions studied are high compared to most apatites and is consistent with the Fe contents observed in apatites considered Fe-bearing (e.g., Franolet and Schreyer 1981; Khudolozhkin et al. 1974). Apatites analyzed from core 6 did not have Fe above detection limits. The average SiO<sub>2</sub> content in apatites from the clay fraction is 1.40 wt%. SiO<sub>4</sub><sup>4-</sup> is known to substitute in apatites but usually involves a coupled substitution with SO<sub>4</sub><sup>4-</sup> (Khorari et al. 1994; Hughes and Drexler 1991; Rouse and Dunn 1982; Sudarsanan 1980). No S was observed above detection limit in the EDS analyses. The lack of measurable fluorine, Si substitution without a coupled sulfate substitution and the comparatively high Fe content makes the apatite clay size fraction unusual with respect to most apatites.

Wavellite commonly occurs as individual or clusters of lath-like crystals and the chemical composition differs from the pure aluminum phosphate end member. Ca, Fe and Si were present with average concentrations of components being CaO (1.57 wt%), Fe<sub>2</sub>O<sub>3</sub> (1.98 wt%), and SiO<sub>2</sub> (5.94 wt%). These concentrations are inconsistent

with those of millisite, a calcium aluminum phosphate that has been commonly reported in phosphate deposits of Florida. Novich and Martin (1989) found wavellite concentrations in clay slimes to vary from 0 to 17% while Zhang and Bogan (1995) found wavellite to be insignificant in the clay tailings (1995). Anderson and Somasundaran (1993) calculated that millisite should be the stable form of phosphate in aged slimes due to the reaction of montmorillonite clays with fluorapatite. This finding is inconsistent with the mineral assemblage observed in the present investigation.

#### Implications for reprocessing

In all the phosphate mineral particles investigated in the clay-sized fraction no fluorine was found above detection limit (approximately 0.1 wt%), nor was any uranium, radium, heavy metal, or REE element detected. Fluorine content in phosphate particles in the sand fraction however are commonly several weight percent and this is consistent with other compositions from phosphatic sands mined in the Florida (Hawkins 1973). This is of environmental significance because one by-product of processing such phosphate ore is hydrofluoric acid (HF) vapors. HF is a well recognized dangerous chemical that produces severe nerve damage and can potentially cause death, even in small quantities. If the clay zone materials were to be reprocessed for phosphate, there may be significantly lower HF emissions compared to common sand-rich ore, at least for the deposit investigated here. This parameter may be important for factoring in life cycle assessment of this and similar ores. If technological and engineering issues can be resolved, the phosphate in this particular tailing deposit may be suitable for reprocessing/recycling as fluorine, heavy metals, and uranium are below detection limits in the clay size fraction. Detailed radiological and heavy metal investigations at the bulk level should be made before reprocessing of this deposit is attempted.

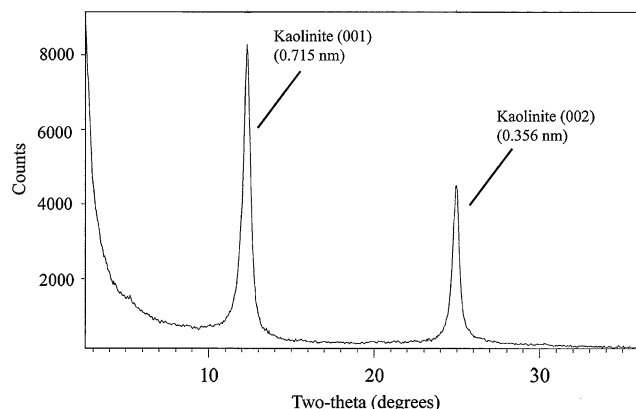
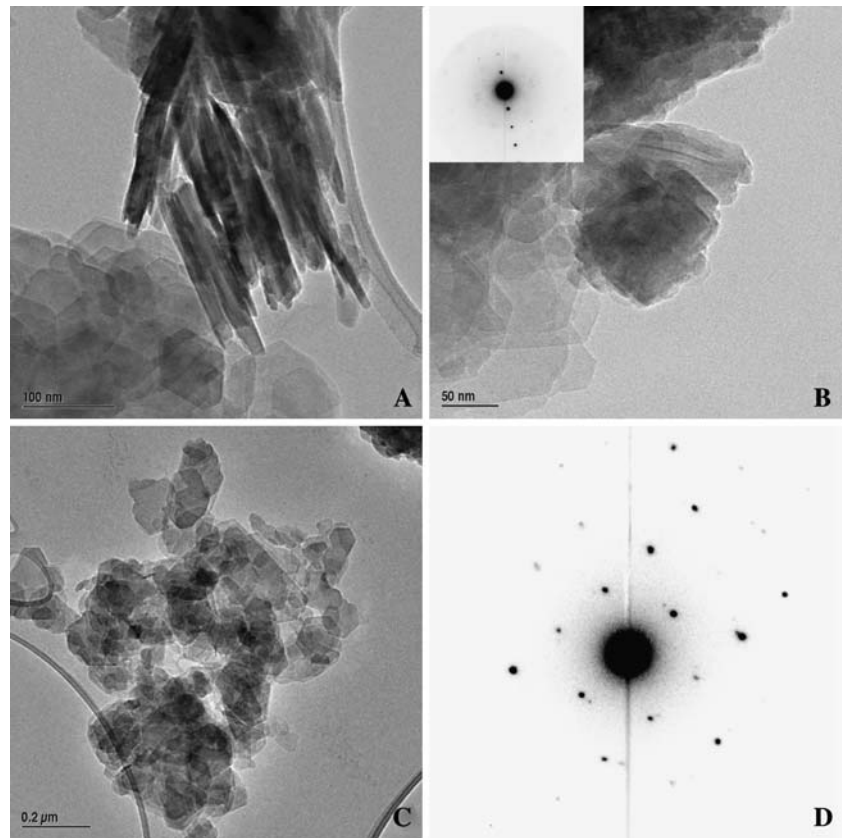


**Fig. 13** A representative X-ray diffraction pattern of kaolinite liner showing sharp well defined peaks of the (001) and (002) reflections

**Fig. 14** **a** TEM image of kaolinite particles from the liner in core 2. *Upper center* showing kaolinite particles on edge with thickness, ~10 to ~35 nm. *Lower left corner* shows kaolinite plates that are euhedral that vary in size, ~80 to ~150 nm. **b** Shows small grain of wavellite in center of image. **c** TEM image of an aggregate of subhedral to euhedral kaolinite platelets. Dimensions vary between 0.15 to 0.05  $\mu\text{m}$ . This texture is very common in the kaolinite liner. **d** SAED pattern showing (hk0) net of center triangular crystals showing high degree of order



The concentration of  $\text{P}_2\text{O}_5$  in bulk sediment varies from approximately 4 to 21 wt% with an average of 14 wt%. Based on this average and assuming an average thickness of 7.5 m and subtracting moisture content there is an estimated 21,000 metric tons of phosphate in bulk sediment of the deposit. Assuming market value of \$1,000 to \$1,600 US per ton the value of phosphate is between approximately \$21 and \$33.6 million.

The concentration of  $\text{P}_2\text{O}_5$  in bulk sediment observed in this investigation is consistent with previous investigations that found a large proportion of phosphate in the ore is lost in the clay slurry waste process. Zhang and Bogan (1995) estimate that one third of the phosphate in the original ore matrix lies in the clay tailings. Older deposits are suspected to contain higher levels of phosphate compared to today's clay settling areas due to improved beneficiation processes. The clay slimes produced in 1954 are estimated to contain 20% phosphate compared to the range of 4.6–17.9% phosphate content for slimes currently produced (Zhang and Bogan 1995). Zhang and Bogan (1995) found that phosphate was distributed fairly evenly among the size fractions, while Hawkins (1973) found apatite to be concentrated in the silt and 2.0–0.2  $\mu\text{m}$  clay fractions. The current investigation indicates that phosphate for this deposit is largely

in apatite in the clay size fraction and is commonly between 50 nm and 2.0  $\mu\text{m}$  in diameter.

Several previous researchers have investigated processes by which the phosphate can be recovered from the clay tailings and include leaching, calcining, or hydroseparation or a combinations thereof. One non-viable method involves leaching the clays with sulfuric acid, then recovering the phosphate from the acid leachate using amine and alcohol (Zhang and Bogan 1995). This method is chemical intensive and large quantities of acid are consumed in the process. The overall reaction is inefficient owing to adsorption and unwanted chemical reactions with clay minerals. Furthermore the technique has an undesired effect of leaching aluminum and iron and therefore requires an additional purification step to produce uniform quality product. Another method of recovering the phosphate requires the dewatering of the clays followed by calcining at 870–1,093°C (Zhang and Bogan 1995). Both dewatering and calcining are extremely energy intensive and therefore not cost effective for phosphate production alone. The most promising investigations to date involve hydrocyclones. Hydroseparators can segregate the clays into size fractions and then flotation can be performed on the coarser material. This process has been found to retrieve 30% of the phosphate from the clay tailings, but still only recovers the

portion of phosphate in the coarser fraction (Zhang and Bogan 1995). This method is not appropriate for this deposit because of the high percentage of apatite in the clay fraction.

#### Implications of mineralogy for restoration

The mechanical stabilization of the clay tailings is a major problem for reclamation and restoration. The use of lime for stabilization of expanding clays or soils has been extensively investigated in a number of settings (e.g., Rogers et al. 2006; Mubeen 2005; Parsons and Milburn 2003; Bartlett and Farnsworth 2002; Tremblay et al. 2001; Nalbantoglu and Gucbilmez 2001; Prusinski and Bhattacharja 1999; Basma et al. 1998; Conner and Hoeffner 1998). This involves equilibration of lime with soil moisture in part to produce  $\text{Ca}^{2+}$  cations that can exchange in interlayer sites of expandable clays such as montmorillonite. Fly-ash used discretely or in combination with lime has also been implemented as a soil stabilizer (e.g., Mohamedi et al. 2007; Parsons and Milburn 2003; Nalbantoglu and Gucbilmez 2002, 2001; Conner and Hoeffner 1998; Indraratna et al. 1995, 1991). Other alternative techniques have been investigated including acids, ionic solutions, enzymes, polymers, resins, petroleum emulsions and lignosulfates (Tingle and Santoni 2003; Rauch et al. 2002) or use of ionic solutions (Katz et al. 2001; Basma et al. 1998). Okagbue (2007) investigated the use of wood ash as a stabilizing agent.

Despite this extensive body of work, detailed investigations of stabilization of phosphatic clays from mine waste tailings are lacking. The results of EDS investigation on smectite particles indicates that there is a wide range of chemical variation in the particles with respect to total  $\text{Fe}_2\text{O}_3$  and  $\text{Al}_2\text{O}_3$  content. Accordingly such variation likely causes variation in the layer charge of the 2:1 layer of the smectites. Substitutions of  $\text{Al}^{3+}$  in octahedral sites and tetrahedral sites produce different types of layer charge which affects expansion behavior and cation exchange capacity. This variation makes the effectiveness of injection of  $\text{Ca}^{2+}$  solutions or other solutions questionable. Furthermore the average concentration of CaO in the smectites is 1.23 wt% and the Ca is commonly found as an interlayer cation. The kinetic mechanisms for exchange may be impeded and exchange with  $\text{Ca}^{2+}$  solutions may be limited and thus might not be an effective technique for soil stabilization.

Permeability is another fundamental problem that exists in using  $\text{Ca}^{2+}$  solutions to stabilize the tailings. Kolstad et al. (2004) investigated permeability of montmorillonite-rich materials exposed to ionic strengths between 0.05 and 0.5 M and showed that the permeability is usually no

greater than  $10^{-7}$  cm/s. Lee and Schackelford (2005) investigated bentonite, with a high montmorillonite content of 86% and similarly showed the material had a low permeability in  $\text{CaCl}_2$  solutions. Both of these investigations showed that the liners remained intact and did not degrade.  $\text{Ca}^{2+}$ -rich solutions injected into the clay may be a possible mechanism to stabilize the clay tailings but the low permeability of the materials is likely problematic. Using the  $10^{-7}$  cm/s as a permeability coefficient and 7.5–9.5 m of the clay tailings as a thickness, a simple linear approximation indicates that migration times for surface application of solutions to move through the deposit investigated would be approximately 230–300 years. Although this is a rough approximation it is indicative that  $\text{Ca}^{2+}$ -rich solution injection appears to not be a viable option for immediate stabilization.

Heavy metals are a major factor in plant health in wetland and associated plants and can be toxic (e.g., Banks et al. 2006; Yongpisanphop et al. 2005; Ali et al. 2004; Odjegba and Fasid 2004; Hui 2002; Carbonell et al. 1998; Zayed et al. 1998; Debusk et al. 1996; Crowder 1991). The clay tailing investigated in this study have appreciable concentrations of V, Cr, and Pb. Common symptoms of heavy metal toxicity associated with Pb and Cr in plants include withering and root color changes. For some plants Pb can cause leaf chlorosis and Cr can cause leaf necrosis (e.g., Yongpisanphop et al. 2005). V and Cr are strongly correlated to apatite. Apatite has a comparatively low solubility. Rakovan (2002) reviewed solubility product constants for apatite and found  $K_{sp}$  values that vary from  $1 \times 10^{-88.5}$  to  $1 \times 10^{-55.9}$  for hydroxyapatite. Therefore although appreciable amounts of V and Cr occur in the apatite at the trace level they are in a phase which is sparingly soluble.

Pb does not clearly correlate to apatite. The distribution of Pb may be controlled by phyllosilicates. Pb may be held as interlayer cations in smectite and palygorskite. Pb is well recognized as having an affinity for sorption with montmorillonites (e.g., Yan et al. 2007; Al-Degs et al. 2006; Bhattacharyya and Sen Gupta 2006; Jozja et al. 2006; Abollino et al. 2003). Gu and Evans (2007) have modeled Pb sorption on the Fithian illite and Pb has also been shown to absorb to palygorskite (Chen and Wang 2007; Potgieter et al. 2006). Pb may be distributed among both montmorillonite and palygorskite as well as being in apatite. If Pb is in the phyllosilicate minerals then it may be more available to plants and pose a toxicity problem for long term ecological restoration.

#### Conclusions

This study is the first extensive investigation of aged clay tailings in Florida and provides fundamentally new details

regarding variation in mineralogy and bulk properties. The results of this study can be used to better understand problems associated with restoration and reclamation. Although there appears to be no systematic distribution of mineral content or water content in the deposit, the nature of the mineralogy and chemical composition of minerals, and variation in water content and organic content is now constrained. This study can be used for comparative purposes for older and younger deposits. The assessment of the nature of phosphate content provides a basis for further economic analysis.

Detailed investigations such as this should be done for similar deposits produced over the span of historical phosphate mining in Florida so as to have a broad understanding of the regional variability of clay tailings. Through a better understanding of mineralogy of the deposits long term management issues may be improved or resolved.

## References

- Abollino O, Aceto M, Malandrino M, Sarzanini C, Mentasti E (2003) Adsorption of heavy metals on Na-montmorillonite: effect of pH and organic substances. *Water Res* 37:1619–1627
- Akhavan-Niaki AN (1961) Contribution à l'étude des substitutions dans les apatites. *Ann Chim* 6:51–79
- Al-Degs YS, El-Barghouthi MI, Issa AA, Khraish MA, Walker GM (2006) Sorption of Zn (II), Pb (II), and Co (II) using natural sorbents: equilibrium and kinetic studies. *Water Res* 40:2645–2658
- Ali NA, Bernal MP, Ater M (2004) Tolerance and bioaccumulation of cadmium by *Phragmites australis* grown in the presence of elevated concentration of cadmium, copper and zinc. *Aqu Bot* 80:163–176
- Andersen JB, Somasundaran P (1993) The role of changing surface mineralogy on the separation of phosphatic clay waste. *Intl J Mineral Process* 38:189–203
- Andrews RL, Broome SW (2006) Oak flat restoration on phosphate-mine spoils. *Restor Eco* 14:210–219
- Banks E, Jaunarajs KL (1965) Chromium analogs of apatite and spodiosite. *Inorg Chem* 4:78–83
- Banks E, Greenblatt M, McGarvey Br (1971) Electron spin resonance of  $\text{CrO}_4^{3-}$  in chlorapatite  $\text{Ca}_5(\text{PO}_4)_3\text{Cl}$ . *J Solid State Chem* 3:308–313
- Banks MK, Schwab AP, Henderson C (2006) Leaching and reduction of chromium in soil affected by soil organic content and plants. *Chemosphere* 62:255–264
- Bartlett S, Farnsworth C (2002) Performance of lime cement-stabilized soils for the I-15 reconstruction project—Salt Lake City, Utah. *Soil mechanics 2002 transportation research Record* (1808), pp 58–66
- Basama AA, Al-Rawas AA, Al-Saadi SN, Al-Zadjali TF (1998) Stabilization of expansive clays in Oman. *Env Eng Geosci* 4:503–510
- Bhattacharyya KG, Sen Gupta S (2006) Pb(II) uptake by kaolinite and montmorillonite in aqueous medium: Influence of acid activation on clays. *Colloids Surfaces A Phys Eng Asp* 277:191–200
- Bloss FD (1997) Crystallography and crystal chemistry. Mineralogical Society of America
- Bradley WI (1940) Structure of attapulgite. *Am Mineral* 25:405–410
- Brown MT (2005) Landscape restoration following phosphate mining: 30 years of co-evolution of science industry and regulation. *Eco Eng* 24:309–329
- Carbonell AA, Aarabi MA, DeLaune RD, Gambrell RP, Patrick WH (1998) Arsenic in wetland vegetation: availability, phytotoxicity, uptake and effects on plant growth and nutrition. *Sci Total Environ* 217:189–199
- Chen H, Wang AQ (2007) Kinetic and isothermal studies of lead ion adsorption onto palygorskite clay. *J Col Int Sci* 307:309–316
- Conner JR, Hoeffner SL (1998) A critical review of stabilization/solidification technology. *Crit Rev Environ Sci Technol* 28:397–462
- Crowder A (1991) Acidification, metals, and macrophytes. *Environ Pollut* 71(2–4):171–203
- Dai Y, Hughes JM (1989) Crystal structure refinements of vanadinite and pyromorphite. *Can Mineral* 27:189–192
- Das BK (1999) Environmental pollution of Udaisager lake and impact of phosphate mine, Udaipur, Rajasthan, India. *Env Geol* 38:244–248
- Debusk TA, Laughlin RB, Schwartz LN (1996) Retention and compartmentalization of lead and cadmium in wetland microcosms. *Water Res* 30:2707–2716
- Engel G, Kreig F, Reif G (1975) Mischekristallbildung und kationeordnung im system bleihydroxylapatit-calciumhydroxylapatit. *J Solid State Chem* 15:117–126
- Erwin KL, Doherty SJ, Brown MT, Best GR (eds) (1997) Evaluation of constructed wetlands on phosphate mined lands in Florida. Florida Institute of Phosphate Research
- Fessler AJ, Moller G, Talcott PA, Exon JH (2003) Selenium toxicity in sheep grazing reclaimed phosphate mining sites. *Vet Human Tox* 45:294–298
- Ford RD, Robbins JM, Werner JT, Cowherd D, Gordon CN, Warmack WB, Brown MM, Monroe KW, George WG, Sanders T, Basch M (1990) Soil survey of polk County, Florida. United States Department of Agriculture, Soil Conservation Service
- Fransolet A-M, Schreyer W (1981) Unusual iron bearing apatite from a garnetiferous pegmatoid, Northampton Block Western Australia. *N Jahrb Mineral Monatsh* 1981:317–327
- Ghose MK (2003) Indian small-scale mining with special emphasis on environmental management. *J Cleaner Prod* 11:159–165
- Gionis V, Kacandes GH, Kastiris ID, Chryssikos GD (2006) On the structure of palygorskite by mid- and near-infrared spectroscopy. *Am Mineral* 91:1125–1133
- Gu XY, Evans LJ (2007) Modelling the adsorption of Cd (II), Cu(II), Ni(II), Pb(II), Zn (II) onto Fithian illite. *J Col Int Sci* 307:317–325
- Güven N (1988) Smectites. In: Bailey SW (ed) *Hydrous phyllosilicates. Reviews in mineralogy*, 19, Mineralogical Society of America, pp 495–576
- Güven N, Delacallerie JBD, Friapat JJ (1992) The coordination of aluminum ions in the palygorskite structure. *Clays Clay Minerals* 40:457–461
- Hawkins WH (1973) Physical, chemical, and mineralogical properties of phosphatic clay slimes from the bone valley formations. MS, University of Florida, Gainesville
- Heijligers HJM, Verbeeck RMH, Driessens FCM (1979) Cation distribution in calcium-strontium-hydroxyapatites. *J Inorg Nuclear Chem* 41:763–764
- Hughes JM, Drexler JW (1991) Cation substitution in the apatite tetrahedral site: crystal structures of type hydroxyllellstadite and type ferromite. *N Jahrb Mineral Month* 7:327–336
- Hughes JM, Cameron M, Crowley KD (1991) Ordering of divalent cations in apatite structure: crystal structure refinements of natural Mn- and Sr-bearing apatites. *Am Mineral* 76:1857–1862

- Hui CA (2002) Lead distribution throughout soil, flora, and invertebrate at a wetland skeet range. *J Tox Environ Health A* 65:1093–1107
- Indraratna B, Nutalaya P, Kuganenthira N (1991) Stabilization of a dispersive soil by blending with fly-ash. *Quart J Eng Geol* 24:275–290
- Indraratna B, Balasubramaniam AS, Khan MJ (1995) Effect of fly-ash with lime and cement on the behavior of a soft clay. *Quarterly J of Eng Geol* 28:131–142
- Jasiniski SM (2007) Phosphate Rock Minerals Yearbook. United States Geological Survey, pp 120–121
- Jones B, Galán, E (1988) Sepiolite and palygorskite. In: Bailey SW (ed) *Hydrous Phyllosilicates. Reviews in Mineralogy*, 19, Mineralogical Society of America, pp 631–674
- Jozja N, Baillif P, Touray JC, Muller F, Clinard C (2006) Incidence of lead uptake on the microstructure of a (Mg, Ca)-bearing bentonite (Prrenjas, Albania). *Europ J Mineral* 18:361–368
- Katz LE, Rauch AF, Liljestrand HM, Harmon JS, Shaw KS, Albers H (2001) Mechanisms of soil stabilization with liquid ionic stabilizer. *Geomaterials* 2001, *Transport Res Rec* 1757:50–57
- Khattech I, Jemal M (1997) Thermochemistry of phosphate products II: Standard enthalpies of formation and mixing of calcium and strontium fluorapatites. *Thermochim Acta* 298:23–30
- Khorari S, Cahay R, Rulmont A, Tarte P (1994) The coupled isomorphic substitution  $2(\text{PO}_4)^{3-} = (\text{SO}_4)^{2-} + (\text{SiO}_4)^{4-}$  in synthetic apatite  $\text{Ca}_{10}(\text{PO}_4)_6\text{F}_2$ : a study by X-ray diffraction and vibrational spectroscopy. *Eur J Solid State Inorg Chem* 31:921–934
- Khudolozhkin VO, Urusov VS, Kurash VV (1974) Mössbauer study of the ordering of  $\text{Fe}^{2+}$  in the fluor-apatite structure. *Geochem Intl* 11:748–750
- Kolstad DC, Benson CH, Tuncer BE (2004) Hydraulic conductivity and swell of nonprehydrated geosynthetic clayliners permeated with inorganic solutions. *J Geotech Geoenviron Eng* 130:1236–1249
- Komnitsas K, Kontopoulos A, Lazar I, Cambridge M (1998) Risk assessment and proposed remedial actions in coastal tailings disposal sites in Romania. *Minerals Eng* 11:1179–1190
- Kreidler ER, Hummel FA (1970) The crystal chemistry of apatite: structure fields of fluor- and chlorapatite. *Am Mineral* 55:170–184
- Krekeler MPS (2004) Improved constraints on sedimentary environments of palygorskite deposits of the Hawthorne Formation, southern Georgia from a detailed study of a core. *Clays Clay Min* 52:253–262
- Krekeler MPS, Guggenheim S (2007) Defects in microstructure in palygorskite-sepiolite minerals: A transmission electron microscopy (TEM) study. *Appl Clay Sci* doi:10.1016/j.clay.2007.05.001
- Krekeler MPS, Guggenheim S, Rakovan J (2004) A microtexture study of palygorskite-rich sediments from the Hawthorne Formation, southern Georgia by transmission electron microscopy and atomic force microscopy. *Clays Clay Min* 52:263–274
- Krekeler MPS., Hammerly E, Rakovan J, Guggenheim S (2005) Microscopy studies of the Palygorskite to Smectite Transformation. *Clays Clay Min* 53:94–101
- LaFevers JR, Brown LA, Fountain RC (1977) A case study of surface mining and reclamation planning. International Minerals and Chemical Corporation, prepared for United States Geological Survey, Integrated Mined Area Reclamation and Land Use Planning 3B
- Lee J, Shackelford CD (2005) Impact of bentonites quality on hydraulic conductivity of geosynthetic clay liners. *J Geotech Geoenviron Eng* 131:64–77
- Mars JC, Crowley JK (2003) Mapping mine wastes and analyzing areas affected by selenium-rich water runoff in southeast Idaho using AVIRIS imagery and digital elevation data. *Rem Sens Env* 84:422–436
- Mendez L, Palacios E, Acosta B, Monsalvo-Spencer P, Alvarez-Castaneda T (2006) Heavy metals in the clam *Megapitaria squallida* collected from wild and phosphorite mine-impacted sites in Baja California, Mexico—considerations for human health effects. *Biol Trace Elem Res* 110:275–287
- Mohamedi AMO, Hossein M, Hassani FP (2007) Evaluation of newly developed aluminum, lime and fly ash technology for solidification/stabilization of mine tailings. *J Math Civil Eng* 19:105–111
- Moore DM, Reynolds RC (1997) X-ray diffraction and analysis of Clay Minerals. Oxford University Press, Oxford
- Mubeen MM (2005) Stabilization of soft clay in irrigation projects. *Irrig Drain* 54:175–187
- Nalbantoglu Z, Gucbilmex E (2001) Improvement of calcareous expansive soils in semiarid environments. *J Arid Environ* 47:453–463
- Nalbantoglu Z, Gucbilmex E (2002) Utilization of an industrial waste in calcareous expansive clay stabilization. *Geotech Test J* 25:78–84
- Norrish K (1954) Crystalline swelling of montmorillonite. *Nature* 173:255–257
- Novich BE, Martin T (1989) Rheology and mineralogy as related to engineering properties of phosphatic tailings. *Int J Mineral Process* 26:205–221
- Odjegba VJ, Fasid IO (2004) Accumulation of trace elements by *Pistia stratiotes*: implications for phytoremediation. *Ecotox* 13:637–646
- Okagbue CO (2007) Stabilization of clay using woodash. *J Math Civil Eng* 19:14–18
- Pan Y, Fleet ME (2002) Compositions of the apatite-group minerals: substitution mechanisms and controlling factors In: Kohn MJ, Rakovan J, Hughes JM (eds) *Phosphates—geochemical, geobiological, and materials importance. Reviews in Mineralogy & Geochemistry*, 48, Mineralogical Society of America, pp 14–49
- Parsons RL, Milburn JP (2003) Engineering behavior of stabilized soils. *Geomaterials* 2003, *Transport Res Rec* 1837:20–29
- Pierce RH, Wetzel DL, Esteves ED (2004) Charlotte harbor initiative: assessing the ecological health of Southwest Florida's Charlotte Harbor Estuary. *Ecotoxic* 13:275–284
- Potgieter JH, Potgieter-Vermaak SS, Kalibantonga PD (2006) Heavy metals removal from solution by palygorskite clay. *Minerals Eng* 19:463–470
- Prusinski JR, Bhattacharja S (1999) Effectiveness of Portland cement and lime in stabilizing clay soils. Seventh international conference on low volume roads 1999 *Transport Res Rec* 1652:215–227
- Rakovan J (2002) Growth and surface properties of apatite. *Phosphates: geochemical, geobiological and materials importance. Rev Mineral Geochem* 48:51–86
- Rate of Reclamation (2005) Report Florida Environmental Protection Bureau of Mine Reclamation. 11p
- Rauch AF, Harmon JS, Katz LE, Liljestrand HM (2002) Measured effects of liquid soil stabilizers on engineering properties of clay. *Geomaterials* 2002, *Transport Res Rec* 1787:33–41
- Rogers CDF, Boardman DI, Papadimitriou G (2006) Stress path testing of realistically cured lime and lime/cement stabilized clay. *J Math Civil Eng* 18:259–266
- Rouse RC, Dunn PJ (1982) A contribution to the crystal chemistry of ellestadite and the silicate sulfate apatites. *Am Mineral* 69:920–927
- Ruston BT (1988) Wetland reclamation by accelerating succession. PhD, University of Florida, Gainesville
- Ryser AL, Strawn DG, Marcus MA, Johnson-Maynard JL, Gunter ME, Moller G (2005) Micro-spectroscopic investigation of selenium-bearing minerals from the Western US phosphate resource area. *Geochem Trans* 6:1–11



- Shang JQ, Lo KY (1997) Electrokinetic dewatering of a phosphate clay. *J Hazardous Mater* 55:117–133
- Singh SP, Ma LQ, Hendry MJ (2006) Characterization of aqueous lead removal by phosphatic clay: equilibrium and kinetic studies. *J Hazardous Mater* B136:654–662
- Srodon J, Eberl D (1984) Illite. In: Bailey SW (ed) *Micas. Reviews in mineralogy*. 13, Mineralogical Society of America, pp 495–544
- Sudarsanan K, Young RA, Wilson AJC (1977) The structure of some cadmium “apatites”  $Cd_5(MO_4)_3X$ : I. Determination of the structures of  $Cd_5(VO_4)_3I$ ,  $Cd_5(PO_4)_3Br$ ,  $Cd_5(AsO_4)_3Br$ ,  $Cd_5(VO_4)_3Br$ . *Acta Crystallogr* B33:3136–3142
- Sudarsanan K (1980) Structure of hydroxyllestadite. *Acta Crystallogr* B36:1636–1639
- Tingle JS, Santoni (2003) Stabilization of clay soils with nontraditional additives. In: Eighth international conference on low volume roads. Transport research record 1819, vols 1 & 2. pp A72–A84
- Tremblay H, Leroueil S, Locat J (2001) Mechanical improvement and vertical yield stress predication of clayey soils from eastern Canada treated with lime or cement. *Can Geotech J* 38:567–579
- Vasan S (1971) Utilization of phosphate slimes. International minerals and chemical corporation, prepared for the environmental protection agency, water pollution control research series
- Verbeeck RMH, Lassuyt CJ, Heijligers HJM, Driessens FCM, Vrolijk JWGA (1981) Lattice parameters and cation distribution of solid solutions of calcium and lead hydroxyapatites. *Calcif Tissue Intl* 33:243–247
- Weber TC (1994) Spatial and temporal simulation of forest succession with implicatios for management of bioreserves. M.S Thesis . University of Florida Gainesville 258p
- Yan LG, Shan MQ, Wen B, Zhang SZ (2007) Effect of lead on the sorption of phenol onto montmorillonites and organo-montmorillonites. *J Colloid Interface Sci* 308:11–19
- Yongpisanphop J, Kruatrachue M, Pokethitiyook P (2005) Toxicity and accumulation of lead and chromium in *Hydrocotyle umbellata*. *J Environ Biol* 26:79–89
- Zayed A, Gowthaman S, Terry N (1998) Phytoaccumulation of trace elements by wetland plants I: Duckweed. *J Environ Qual* 27:715–721
- Zhang P, Bogan M (1995) Recovery of phosphate from Florida beneficiation slimes I. Re-identifying the problem. *Minerals Eng* 8:523–534